

UNIVERSIDAD DE CHILE
FACULTAD DE CIENCIAS FÍSICAS Y MATEMÁTICAS
DEPARTAMENTO DE INGENIERÍA ELÉCTRICA

SYSTEM STRENGTH CONSTRAINED UNIT COMMITMENT IN POWER SYSTEMS WITH HIGH PENETRATION OF INVERTER-BASED RESOURCES

TESIS PARA OPTAR AL GRADO DE MAGÍSTER EN CIENCIAS DE LA INGENIERÍA, MENCIÓN ELÉCTRICA

MEMORIA PARA OPTAR AL TÍTULO DE INGENIERO CIVIL ELÉCTRICO

CRISTÓBAL ESSER AMARO

PROFESOR GUÍA:
RODRIGO MORENO VIEYRA

MIEMBROS DE LA COMISIÓN:
PATRICIO MENDOZA ARAYA
PIERLUIGI MANCARELLA

SANTIAGO DE CHILE

2026

RESUMEN DE LA TESIS PARA OPTAR AL GRADO DE MAGÍSTER EN CIENCIAS DE LA INGENIERÍA, MENCIÓN ELÉCTRICA Y MEMORIA PARA OPTAR AL TÍTULO DE INGENIERO CIVIL ELÉCTRICO
POR: CRISTÓBAL ESSER AMARO
FECHA: 2026
PROFESOR GUÍA: RODRIGO MORENO VIEYRA

SYSTEM STRENGTH CONSTRAINED UNIT COMMITMENT IN POWER SYSTEMS WITH HIGH PENETRATION OF INVERTER-BASED RESOURCES

The increasing penetration of inverter-based resources (IBRs), particularly those operating in grid-following (GFL) mode, poses significant challenges to system strength and stability. This thesis proposes a unit commitment (UC) model that incorporates system strength constraints using the available fault level (AFL) metric, practically adopted by industry, which captures both the weakening effect of GFL units and the strengthening contributions of synchronous generators (SGs) and grid-forming (GFM) battery energy storage systems (BESS). To address the computational complexity of the AFL formulation, a cut-generation algorithm is developed to enable scalability for large-scale systems. Case studies on the northern region of the Chilean Power System demonstrate the influence of AFL constraints on system operation, the relevance of enabling curtailment for meeting AFL requirements, and the value of GFM technologies. The proposed framework offers a practical and scalable solution for secure and cost-efficient operation under high IBR penetration.

RESUMEN DE LA TESIS PARA OPTAR AL GRADO DE MAGÍSTER EN CIENCIAS DE LA INGENIERÍA, MENCIÓN ELÉCTRICA Y MEMORIA PARA OPTAR AL TÍTULO DE INGENIERO CIVIL ELÉCTRICO
POR: CRISTÓBAL ESSER AMARO
FECHA: 2026
PROFESOR GUÍA: RODRIGO MORENO VIEYRA

UNIT COMMITMENT CON RESTRICCIONES DE ROBUSTEZ EN SISTEMAS DE POTENCIA CON ALTA PENETRACIÓN DE RECURSOS BASADOS EN INVERSORES

La creciente penetración de recursos basados en inversores (IBRs), particularmente aquellos que operan en modo seguidor de red (GFL), plantea desafíos significativos para la robustez y estabilidad de los sistemas de potencia. Esta tesis propone un modelo de *unit commitment* (UC) que incorpora restricciones de robustez del sistema utilizando la métrica de nivel de falla disponible (AFL), adoptada por la industria, la cual captura tanto el efecto debilitante de las unidades GFL como las contribuciones a la robustez de los generadores sincrónicos (SGs) y los sistemas de almacenamiento de energía en baterías con control formador de red (GFM-BESS). Para abordar la complejidad computacional de la formulación AFL, se desarrolla un algoritmo de generación de cortes que permite la escalabilidad a sistemas reales. Casos de estudio en la zona del norte grande del Sistema Eléctrico Nacional demuestran la influencia de las restricciones AFL en la operación del sistema, la relevancia de habilitar el vertimiento para cumplir con los requisitos de AFL mínimo y el valor operacional desbloqueado por las tecnologías GFM. El trabajo propuesto ofrece una solución práctica y escalable para una operación segura y costo eficiente de sistemas de potencia con alta penetración de IBRs.

Para mi familia,

esto es gracias a ustedes

Acknowledgment

No puedo comenzar los agradecimientos sin, en primer lugar, agradecerle a mis papás, Rosa y Pablo, por todo el apoyo que me brindaron durante mi formación escolar y universitaria. Ustedes me enseñaron lo que es el esfuerzo, la perseverancia, a nunca rendirse y a terminar lo que uno empieza. Sin estos valores que me inculcaron, esta tesis jamás hubiese visto la luz. También agradecerles a mis hermanos, Gabriel y Valentín, quienes son y serán por siempre mis compañeros de vida. Una mención honrosa para el *Toni*, que es el primero que me sale a recibir cuando llego a la casa, solamente esperando a cambio un paseo por la plaza.

Como no también agradecerles a mi *Mama* y a mi *Tata*, quienes siempre me han recibido con la sonrisa y el abrazo más cariñoso. Siempre estaré agradecido que tengan un espacio en su mesa para mí, con el plato de comida más rica y reconfortante que pueda existir. No sé como agradecerles todo lo que han hecho por mí y estaré siempre en deuda con ustedes.

Una dedicación especial para mi compañera de vida Isidora, quien me acompañó en prácticamente toda mi vida universitaria. Gracias a ti podía despejarme los fines de semana y no estar atrapado pensando todo el rato en los controles, las tareas y la tesis. Te amo y sé que pase lo que pase, nuestros caminos están destinados a estar juntos. Gracias por todo.

Quiero agradecer también a toda mi familia, los Esser y los Amaro, por estar siempre ahí. En especial a mi tía Carola, siempre siendo la más *lolein* y estando en todos los cumpleaños y celebraciones. Agradecer también al *Coco*, por tenerme siempre toda la fe del mundo y hacer que me crea el cuento. Aunque no seamos familiares de sangre, quiero agradecer al *Luchito*, mi padrino, por siempre apoyarme y haber estado dispuesto a que sea su ahijado. Un beso y un abrazo al cielo a mi tío Juan, que partió durante mi etapa universitaria. Te quiero y te extraño cada día.

Un agradecimiento a mis amigos del colegio: Seba, Andrés, Benja, Tomás, Salinas, Visho, Felipe y Cristian; porque a pesar de que no nos juntamos tantos como quisiéramos, siguen estando ahí. Agradecer también a mis amigos del Tabo: Calu, Chelo, NZ, Lyon, Al, Pao, Hanna, Troy, Migue, Castt y Pipe por todas las risas y buenos momentos en la etapa de la u. Le doy las gracias a mis amigos de eléctrica Pablo y Diego, con quienes pasamos todo el insufrible plan común de eléctrica. Por último, pero no menos importante, un agradecimiento a mis amigos de la salita: Osvaldo, CS Kinter, Enzo, Pame, Vatulinho, Yerko, JP y Migue. Gracias por todas las discusiones y apoyo durante la realización de la tesis.

Dedico también a los amigos que hice durante mi estadía en Australia, en especial al Cousin, Shark, Cristian, Pabulo y Roger, quienes fueron un pilar fundamental cuando estuve lejos de casa.

Finalmente, agradecer a mis profesores, en especial a Rodrigo por haber aceptado ser mi profesor guía y a la profe Claudia por introducirme en el desafiante mundo de los sistemas de potencia. Estoy sumamente agradecido de todas sus enseñanzas, tiempo dedicado y excelente disposición.

Table of content

1 Introduction 1

1.1 Motivation 1
1.2 Hypothesis 2
1.3 Objectives 2
1.3.1 General objective 2
1.3.2 Specific objectives 3
1.4 Structure of the document 3

2 Literature review 4

2.1 System strength 4
2.1.1 Impact of IBRs on system strength 4
2.1.2 System strength metrics 5
2.2 Experiences and practices in operating power systems considering system strength criteria 8
2.2.1 Approaches by system operators 9
2.2.2 State of the art in UC models with system strength constraints 10

3 Methodology 15

3.1 Definition of parameters, variables and sets 15
3.2 Development of AFL-constrained UC model 16
3.2.1 Model overview 16
3.2.2 Objective function 17
3.2.3 Transmission constraints and balance equation 17
3.2.4 SG constraints 18
3.2.5 Renewable generation constraints 19
3.2.6 BESS constraints 19
3.2.7 AFL constraints 19
3.3 Development of solution algorithm 21

4 Results and analysis 24

4.1 System characterization and input data 24
4.2 Performance of the proposed model 27
4.3 Analysis on system operation 29
4.4 Impact of enabling AFL-driven curtailment 30
4.5 Comparison with conventional security constraints 32
4.6 Analysis on future system scenarios 33
4.7 Performance of the cut-generation algorithm 36

5 Conclusions 38

5.1 Future work 38

Bibliography 40
Annex A. PTDF matrix calculation 45
Annex B. YGFM matrix properties 47
Annex C. Techno-economic parameters of SGs and BESS 48

List of figures

Figure 3.1: Diagram of cut-generation algorithm. n denotes the iteration number. 23
Figure 4.1: (a) Map of the CPS. (b) Installed capacity in the CPS by region and technology. 24
Figure 4.2: Graph representation of the NG region. 25
Figure 4.3: Renewable and demand profiles for NG region in the CPS. 26
Figure 4.4: (a) Representation of the rest of the CPS. (b) Power flow and SCL profiles at the interconnection bus between the NG region and the rest of the system. 27
Figure 4.5: Minimum AFL in the NG region throughout the day with classical and proposed UC models. 28
Figure 4.6: (a) Number of committed SGs for each case study. (b) Percentage of time SGs units are on by technology 30
Figure 4.7: Percentage of time SGs units are on by technology comparison when enabling AFL-driven curtailment and without enabling it. 31
Figure 4.8: Daily operating cost for different conventional security-constraints. (a) Minimum inertia constraint. (b) Minimum number of online SGs required. (c) Maximum non-synchronous penetration. 34
Figure 4.9: Daily operating cost vs different levels of installed renewable capacity for different system configurations: No BESS (red line), BESS-GFL (blue line) and BESS-GFM with overloading capacity of 1.0 p.u. (green line), 1.5 p.u. (orange line) and 2.0 p.u. (purple line). (a) Scenario with coal-fired units. (b) Scenario with coal-fired units fully decommissioned. (c) Scenario with coal-fired units replaced by SCs. 35

List of tables

Table 2.1: Comparison between system strength metrics. 7
Table 2.2: Comparison of reviewed works..... 13
Table 4.1: Daily operating cost with classical and proposed UC model. 29
Table 4.2: Daily renewable curtailment with classical and proposed UC model. 29
Table 4.3: Daily operating cost comparison with and without enabling AFL-driven curtailment.31
Table 4.4: Daily renewable curtailment comparison with and without enabling AFL-driven curtailment. 31
Table 4.5: Objective value and solving time obtained in each iteration when solving the AFL-constrained UC model using the cut-generation algorithm. 37
Table C.1: Techno-economic parameters of existing SGs. 48
Table C.2: Techno-economic parameters of existing SGs (continuation)..... 49
Table C.3: Technical parameters of BESS. 50

1 Introduction

1.1 Motivation

Due to the growing urgency to reduce carbon emissions in response to global warming, countries worldwide have strongly promoted the deployment of unconventional renewable energy sources for electricity generation. As a result, power systems are undergoing an energy transition characterized by an increasing penetration of Inverter-Based Resources (IBRs), such as photovoltaic solar, wind generation, and Battery Energy Storage Systems (BESS). Chile exemplifies this transition: as of March 2025, the Chilean Power System (CPS) had a total installed capacity of approximately 37,395 MW, of which around 18,990 MW (about 50.8%) came from IBRs [1], reflecting their significant deployment. In this context, Chile has set a target to retire all coal-fired power plants by 2040; consequently, the penetration of IBRs in the CPS is expected to continue increasing in the coming years [2].

While the integration of IBRs brings significant environmental and economic benefits, it also introduces critical challenges for power system stability and security. One of the most pressing issues is the reduction in system strength, a property that reflects the ability of the grid to maintain stable voltages under disturbances and variations in power flows [3]. Traditionally, the strength of a system at a bus can be measured according to the Short-Circuit Level (SCL) at that location. High SCL are generally found in strong power systems, while low SCL are representative of weak power systems. SGs can inject large short-circuit currents, while the contribution that IBR can deliver is limited to protect power electronics. In fact, during a fault, IBR plants contribute short-circuit currents between 1.1-1.5 [p.u.] [4], while SGs can inject up to 6 or 9 times their rated current [5]. Therefore, SCL in areas with a high concentration of IBR and scarce synchronous generation are very low. Moreover, most IBR operate in Grid-Following (GFL) mode, which need strong voltages at their Point of Connection (PoC) to follow the voltage changes for a correct synchronization with the grid [6]. Then, as SGs are displaced by GFL-IBRs, fault current levels and voltage stiffness decline, increasing the risk of instability, particularly in weakly meshed networks or regions with concentrated renewable generation.

Weak power systems are complex systems, difficult to control, and have a higher risk of experiencing unstable behaviours [7]. In a weak system with low SCL, voltages are very sensitive to changes in operating conditions, meaning that small changes in power flows lead to significant voltage variations in the system [8]. In the same way, significant voltage drops can lead to significant accelerations in the rotors of SGs, which can trigger a loss of synchronism [9]. In this sense, stability problems in weak systems can manifest themselves in different ways, including classical problems such as voltage instability and loss of synchronism of SGs. Additionally, various studies and practical experiences have shown that weak power systems can also present stability issues associated with the control of IBR, which are characterized by having fast dynamics compared to the electromechanical dynamics of conventional systems [10], [11].

To address stability issues, network operators conduct various studies to identify preventive measures that allow maintaining safety even under critical operating conditions. However, the

complexity of stability studies in real power systems has led to them being carried out only for a limited set of scenarios selected according to the worst-case scenario criterion [12]. Consequently, these studies generally result in a set of operational constraints based on heuristics that, while they allow maintaining a certain margin of safety, tend to be quite conservative and, most of the time, unjustified.

System operators around the world have incurred in different practices to address system strength shortfalls. For example, the Chilean system operator enforces minimum inertia constraints in order to commit additional SGs to provide SCL [13]. On the other hand, the Australian Energy Market Operator (AEMO) requires a minimum number of SGs that must remain online to operate the system with adequate system strength levels [14]. Finally, the Irish system operator also includes a minimum number of online SGs requirement as well as a maximum limit for non-synchronous penetration, which constraints the active power injection from GFL-IBRs [15], [16]. However, these constraints are often heuristic and system-wide, failing to capture the local nature of system strength. These measures can lead to inefficient Unit Commitment (UC) decisions, inefficient renewable curtailment, and increased operational costs. Moreover, they overlook emerging technologies like Grid-Forming (GFM) BESS, which can provide system strength services without relying on synchronous generation.

This context motivates the need for advanced UC models that explicitly incorporate system strength constraints into day-ahead planning. By doing so, system operators can ensure secure operation while minimizing costs and enabling higher renewable integration. Furthermore, such models can unlock the value of technologies capable of enhancing system strength, paving the way for more efficient low-carbon power systems.

1.2 Hypothesis

This research hypothesizes that incorporating system strength constraints —expressed through the Available Fault Level metric— into the unit commitment problem enables cost-efficient operation of power systems with high penetration of inverter-based resources while maintaining adequate levels of system strength. By explicitly modelling the contribution of synchronous generators and grid-forming batteries, the proposed approach will outperform conventional heuristic constraints (e.g., minimum inertia or synchronous unit requirements) in terms of operational cost and renewable integration.

1.3 Objectives

1.3.1 General objective

To develop and implement a unit commitment optimization framework that explicitly incorporates system strength constraints based on the Available Fault Level metric, including the development of a mathematical formulation and a scalable algorithm to efficiently solve the resulting model.

1.3.2 Specific objectives

- To develop a mathematical formulation of system strength requirements using the Available Fault Level metric, ensuring compatibility with classical unit commitment models.
- To reformulate the Available Fault Level-constrained unit commitment model into a Mixed-Integer Linear Programming structure through appropriate linearization and approximation techniques to enable efficient solution for large-scale systems.
- To design and implement a scalable solution algorithm that enables the practical resolution of the Available Fault Level-constrained unit commitment model for realistic power systems.
- To incorporate the operational modes of batteries —both grid-following and grid-forming— into the model to evaluate their contribution to system strength and overall operational efficiency.
- To perform case studies to analyze the cost, renewable curtailment, and system strength implications of the proposed methodology under varying renewable penetration levels and coal phase-out conditions.

1.4 Structure of the document

The remainder of this thesis is organized as follows. Chapter 2 presents a comprehensive literature review covering the concept of system strength, its associated metrics, and current practices adopted by system operators and academia to incorporate system strength criteria into power system operation. Chapter 3 details the methodology of this work, including the formulation of the AFL-constrained unit commitment model and the development of the proposed cut-generation solution algorithm. Chapter 4 introduces the system under study, describes the case-study setup, and presents an in-depth analysis of the results. Finally, chapter 5 summarizes the main conclusions derived from this research and outlines potential directions for future work.

2 Literature review

This chapter begins by introducing the concept of system strength and its relationship to SCL. It then examines the impact of IBRs, considering their operating modes. Subsequently, various metrics for assessing system strength are discussed. The chapter further provides a comprehensive overview of academic and industry practices for power system operation considering system strength criteria.

2.1 System strength

System strength is defined as the sensitivity of voltage to variations in power flows [17]. A strong system is one that can maintain stability during contingencies, as its state variables exhibit minimal deviations under disturbances [3]. Such strength level provides a longer time margin for implementing corrective actions, thereby preventing widespread disconnection of devices and loads [18]. Furthermore, since equipment must operate within specified voltage ranges, it is preferable for devices to be connected to a strong system [19]. This reduces the risk of damage and contributes to extending their operational lifespan.

Traditionally, SCL has been used as a proxy for system strength. A bus with a high SCL is considered strong, as voltage deviations are reduced under disturbances [20], [21]. Increasing SCL requires reducing the Thévenin equivalent impedance seen from a bus [10]. Highly meshed networks with a large number of committed SGs exhibit low Thévenin impedances. SGs are the primary sources of short-circuit current, capable of delivering up to 9 times their nominal current during faults, with typical contributions ranging between three and six times their nominal capacity. Consequently, buses located near SGs have higher SCL, whereas areas distant from synchronous generation centres tend to exhibit lower SCL [18]. In summary, the strength of a bus can be enhanced by committing nearby SGs, thereby reducing its Thévenin impedance.

2.1.1 Impact of IBRs on system strength

IBRs have thermal limitations associated with their semiconductor devices, which restrict their short-circuit current contribution to approximately 1.0-1.2 times their nominal current [18]. This represents a major distinction from synchronous machines, which can supply between 3 and six times their nominal current, and in some cases up to 9 times. Consequently, the displacement of SGs with IBRs leads to a reduction in SCL [22]. However, the influence of IBRs on system strength also depends significantly on their operating mode.

2.1.1.1 Grid-Following IBRs

Most IBRs operate in GFL mode, in which the inverter synchronizes with the voltage phase at its PoC. To achieve this, GFL-IBRs employ a Phase-Locked Loop (PLL) responsible for synchronizing the inverter voltage with the grid voltage [23]. As a result, GFL-IBRs exhibit a delay of approximately 20 ms in their short-circuit current contribution [24]. This characteristic can lead to significant voltage drops during faults at buses located far from SGs. Moreover, studies have shown that GFL-IBRs connected to weak buses may experience instabilities associated with the dynamics of the PLL [18].

Additionally, the interaction between the various control systems of IBRs and the fast dynamics of the transmission network, as well as the electromagnetic phenomena associated with the transient behaviour of SGs stators following a disturbance, can lead to stability issues in weak grids [10], [25]. For example, control-mode instability may occur, resulting in oscillations with increasing amplitude over time or poorly damped oscillations triggered by small system disturbances. In [26], it is shown that for wind turbines connected to a weak grid, poorly damped or even undamped oscillations may arise depending on the network characteristics at the point of connection. If the connection is weak, there is a greater tendency for a pole to appear in the right half-plane of the open-loop transfer function, which translates into an unstable system under small perturbations. This situation also depends on the delay associated with dq-axis current control and the power injected by the inverter into the system [27], [28].

2.1.1.2 Grid-Forming IBRs

Nowadays, IBRs can operate in GFM mode, which can provide system strength despite they have limited fault currents [29]. Unlike GFL-IBRs that must follow the voltage phase at their PoC to synchronize with the grid, GFMs are capable of establishing the voltage and frequency at their connection point [30]. If the switching processes occurring in the semiconductors are not considered and it is assumed that current saturation does not occur, a GFM can be represented as a voltage-controlled source behind an impedance, which sets the internal voltage and frequency. Then, unlike GFL-IBRs, GFM units can inject short-circuit current immediately after a fault occurs [31]. Consequently, GFM-IBRs in operation can effectively reduce the Thévenin impedance seen by the buses, thereby increasing system strength. To effectively contribute to system strength, GFM-IBRs must have sufficient headroom and footroom to operate reliably as voltage sources [3]. Due to this requirement, GFM inverters are primarily being deployed in BESS [32].

2.1.2 System strength metrics

The ability to identify weak areas within power systems is crucial for planning and operating them reliably, as it enables understanding of potential regions where issues related to low system strength may arise. Weak grids and their associated challenges are often system-specific, making general interconnection standards or requirements difficult to apply uniformly [10], [18]. Therefore, system operators have to adopt a variety of tools, techniques, and methodologies to identify weak areas and assess whether more detailed analyses are necessary for each interconnection or for regions susceptible to weak-grid conditions and deep IBR penetration.

Currently, several metrics exist to quantify system strength at a specific point in the system. These indicators serve as useful tools for identifying weak areas within the network. Since low system strength levels are associated with a higher likelihood of stability issues in GFL-IBR units, most metrics focus on assessing the strength of buses where these units are connected. Furthermore, as discussed in the previous section, it is important that a system strength metric accounts for potential interactions among nearby GFL-IBR units and also reflects their operating point (active power output).

2.1.2.1 Short-Circuit Ratio

The most basic and easiest-to-apply metric for determining the relative system strength of a power system is the Short-Circuit Ratio (SCR), which is defined as the ratio between the apparent short-circuit power of a three-phase fault at the PoC of a GFL-IBR and its nominal power [33].

Historically, the SCR has been the most widely used metric for estimating system strength. A grid is considered weak for the connection of a given GFL unit if $2 < SCR < 3$ at the PoC or very weak if $SCR < 2$ [24], [34]. This condition implies that the power system will be more sensitive to active and/or reactive power injections, and therefore, the integration of a new GFL unit may compromise its stability (e.g., voltage dip tolerance, control interactions, control instabilities, etc.). Conversely, a grid is considered strong at the PoC if $SCR > 3$ indicating that the system will have a lower tendency to exhibit instabilities [24], [34]. Despite its widespread use, the SCR has certain limitations in its calculation and application. For instance, when a new GFL-IBR is connected, SCR treats it as an independent unit, even though it may belong to a cluster of several electrically close GFL units that could interact with each other. Therefore, SCR is more appropriate when considering a single GFL-IBR operating in a relatively conventional power system dominated by SGs, without many electrically close GFL units [18].

2.1.2.2 Weighted Short-Circuit Ratio

To account for the effect of interactions among nearby GFL-IBRs and thus provide a better estimation of system strength, the Weighted Short-Circuit Ratio (WSCR) has been proposed [34]. The calculation of WSCR is based on the assumption of strong interactions between adjacent GFL units, which is equivalent to assuming that all units are connected to the same PoC [18], [34]. However, in real systems, there is some electrical distance between units, meaning they will not fully interact with each other. By not considering this electrical separation, WSCR may yield overly pessimistic system strength estimates.

2.1.2.3 Site-Dependent Short-Circuit Ratio

The Site-Dependent Short-Circuit Ratio (SDSCR), proposed in [35], provides a more accurate assessment of system strength by considering the proximity to static voltage stability limits. Unlike traditional metrics, SDSCR accounts for interactions among multiple GFL-IBRs at different sites through the mutual impedances in the impedance matrix. Additionally, it incorporates the actual operating active power injection of GFL units rather than their nominal power, as used in SCR and WSCR.

2.1.2.4 Generalized Short-Circuit Ratio

An alternative approach is the generalized Short-Circuit Ratio (gSCR), proposed in [36], for evaluating the small-signal stability of systems with high penetration of GFL-IBRs. In the gSCR formulation, the admittance model of a GFL-IBR, combined with that of the grid, is represented as a multiple-input multiple-output (MIMO) control loop characterized by a reduced admittance matrix. Then, the small-signal stability of the system depends on whether the eigenvalues of this reduced matrix lie in the left half of the complex plane. These eigenvalues are influenced by the control strategies and parameters of GFL-IBRs, the degree of network meshing, and the number of

voltage sources (SGs and GFM-IBRs) operating in the system [37], [38]. The underlying intuition behind gSCR is that bus voltages must be sufficiently strong —or equivalently, GFL units must be electrically close to voltage sources— so that their PLL can accurately track the grid phase. However, gSCR essentially provides a worst-case assessment of overall system strength, and its applicability to a specific PoC remains unclear [8].

2.1.2.5 Available Fault Level

SCR-based metrics evaluate the strength of buses hosting GFL-IBRs, while the gSCR provides a single value for a whole system. However, a bus can be inherently weak regardless of whether a GFL-IBR is connected to it. To address this, the Available Fault Level (AFL) was proposed in [39] as a metric for assessing the strength of any bus in the system. AFL is calculated as the difference between the SCL provided by GFM units —including SGs and GFM-IBRs— and the SCL 'consumed' by GFL-IBRs. This approach enables consideration of electrical interactions among GFL-IBRs without requiring mutual impedance calculations. Furthermore, in the absence of GFL-IBRs, AFL reduces to the SCL, which remains the traditional proxy for system strength.

2.1.2.6 Comparison of system strength metrics

Each of the metrics described has advantages and disadvantages as a tool for identifying weak areas of the network and, therefore, potential issues related to SCL. Table 2.1 provides a qualitative comparison of these indicators. Ideally, a system strength metric should consider the operating point of GFL-IBR units as well as electrical interactions among these units. Conversely, it is desirable that the metric does not require knowledge of GFL control parameters, since these are typically unavailable in practice due to industrial secrecy. Additionally, the metric should be capable of providing estimates for any bus in the system, allowing system operators the flexibility to select any bus for system strength assessment. Finally, it is preferable that the metric is already used in practice, as this ensures stronger technical support for its application compared to metrics found only in the literature.

From Table 2.1, the AFL defined by CIGRÉ and adopted by AEMO [40], offers a practical and technically robust alternative. While in its definition considers nominal power of GFL-IBRs, can be easily modified to account for the operating point of these units instead. Considering this modification, the AFL can meet all the desirable characteristics as a system strength metric discussed in Table 2.1.

Table 2.1: Comparison between system strength metrics.

	SCR	**WSCR**	**SDSCR**	**gSCR**	**AFL**
Does it consider the operating point of GFL-IBRs?	X	X	✓	✓	X
Does it account for electrical interactions between GFL-IBRs?	X	✓	✓	✓	✓
Does it need control parameters of GFL-IBRs for its calculation?	X	X	X	✓	X

Does it provide a system strength estimation for any bus in the system?	X	X	X	X	✓
Is it used in practice?	✓	✓	X	X	✓

2.2 Experiences and practices in operating power systems considering system strength criteria

Driven by the displacement of SGs with GFL-IBRs power system operation has become significantly more complex. System operators now face the challenge of maintaining adequate levels of system strength while minimizing operational costs. As discussed in the previous section, system strength is closely related to SCL, which primarily depend on the number of committed SGs. Therefore, operators must ensure sufficient system strength when solving the UC problem. However, directly incorporating SCL constraints into the UC formulation is not straightforward, as the relationship between SCL and SG commitment is highly nonlinear. This section reviews approaches adopted by system operators and recent advances in the literature to address this challenge.

2.2.1 Approaches by system operators

Power system operators worldwide have progressively introduced operational security constraints to manage the increasing penetration of GFL-IBRs and the consequent reduction in system strength and SCL. Although the specific implementations differ across systems, a common feature is the explicit enforcement of minimum number of committed SGs and/or limits on non-synchronous penetration.

In the Irish power system, operated by EirGrid and SONI, system security under high renewable penetration is managed through the System Non-Synchronous Penetration (SNSP) metric. SNSP is defined as the ratio between non-synchronous generation (mainly wind, solar, and HVDC imports) and total system demand plus exports. This metric is enforced as a real-time operational constraint to limit the proportion of non-synchronous generation connected to the system [15]. In parallel, the Irish system operators also enforce a minimum number of synchronous units online, reflecting the need to guarantee sufficient inertia, fault current contribution, and voltage control capability [16]. These combined constraints have played a central role in the secure integration of very high shares of wind generation, while at the same time becoming a key driver of renewable curtailment during low-demand and high-wind conditions [41].

In the National Electricity Market (NEM) in Australia, AEMO have adopted a region-specific approach based on minimum SG requirements and system strength obligations. South Australia (SA) represents the most prominent example, as it became the first large-scale power system to operate with instantaneous renewable penetrations above 100%. Following blackouts and system strength concerns, AEMO imposed minimum SG requirements to ensure adequate fault levels. Initially, at least four SGs were required to remain online [42]. After the installation of large Synchronous Condensers (SCs), this requirement was progressively reduced to two units, and under certain network conditions, operation with only one SG has been demonstrated as technically feasible [43]. These requirements are complemented by explicit system strength standards expressed in terms of minimum fault levels at critical network nodes, which transmission operators must satisfy through network reinforcements, SCs, or contractual arrangements with generators [44].

The high generation coming from GFL-IBR units in the northern area of the Chilean national electric system has prompted the system operator to carry out various analyses aimed at preserving adequate levels of system strength. In this context, the system operator imposes minimum inertia restrictions in the northern area in order to commit additional SG units and thus, indirectly, achieves minimum SCL levels in the network [13].

Despite efforts to maintain adequate levels of system strength, these three approaches share a common shortcoming: the constraints imposed by system operators do not explicitly target system strength —whether by ensuring minimum SCL or by meeting any of the metric requirements discussed in the previous section. Moreover, limits on non-synchronous penetration, minimum synchronous unit commitments, or minimum inertia constraints overlook the local characteristics of system strength. As a result, these practices can lead to more costly UC outcomes compared to explicitly incorporating system strength constraints. The challenge, however, lies in

effectively integrating such constraints into UC models, given the highly nonlinear relationship between SG commitment variables and SCL. Consequently, the remainder of this section reviews the state of the art in UC models that include system strength constraints.

2.2.2 State of the art in UC models with system strength constraints

When dealing with systems with high IBR penetration, obtaining an UC output that maintains minimum system strength levels is essential. Since SGs are the primary sources of SCL, ensuring minimum SCL —or meeting any other system-strength criterion— depends strongly on which SG units are committed. However, the relationship between SG commitment decisions and the resulting SCL is highly nonlinear, which calls for specialized solution methodologies to handle it efficiently. This section reviews the state of the art on incorporating system-strength criteria into power system operation models, with a particular focus on the solution methodologies employed.

2.2.2.1 Power system operation models with minimum SCL constraints

Due to the typical relationship between system strength and SCL, one of the earliest strategies involves embedding minimum SCL requirements into UC formulations. A foundational contribution in this area is the work presented by the authors in [45], which introduces a novel approach to integrate fault level requirements into an UC framework. The minimum SCL constraint is defined as in (2.1).

$$\mathrm{K}\mathbf{C}\boldsymbol{u} \geq \mathbf{SCL_{min}} \tag{2.1}$$

Where $\boldsymbol{u}$ contains the commitment decision variables of SGs in each time period. Matrix $\mathbf{C}$ contains the System Strength Contribution Factors (SSCFs), which quantify the SCL that a given SG contributes to a specific bus. $\mathbf{SCL_{min}}$ is the vector of minimum required SCL at designated buses. Finally, K is a scaling factor used to calibrate the SSCFs, acknowledging that the actual contribution of a SG may differ from the value estimated by its corresponding SSCF. However, this scaling factor must be computed iteratively by checking if the real SCL greater or equal than the minimum SCL required. The system used to validate this proposed model corresponded to a reduced representation of the South Australia and Victoria power systems, which comprises 86 SGs—four of which are capable of operating in SC mode—23 wind farms, one BESS, 217 buses and 363 transmission lines [46]. Minimum fault level requirements are imposed at three critical buses in the network.

Another study that incorporates minimum levels of SCL is presented in [47]. Here, the SCL constraint is expressed in terms of the diagonal elements of the impedance matrix, given that SCL is inversely related to these diagonal entries. However, computing the impedance matrix requires inverting the admittance matrix, whose diagonal components depend on binary decision variables (the commitment of SGs). This dependence introduces substantial complexity into the optimization problem. The study compares two linearization methods to achieve a more favourable trade-off between accuracy and computational efficiency: an analytical method and a data-driven approach. In the analytical method, each element of the impedance matrix is treated as a decision variable, whereas only the diagonal elements of the admittance matrix contain decision variables. As a result,

the minimum SCL constraint can be effectively linearized using McCormick relaxations [48]. Nonetheless, the computational burden of solving the analytical formulation remains extremely high. In contrast, the data-driven approach models each impedance-matrix element as a linear combination of SG commitment decisions. The corresponding linear coefficients are obtained by minimizing the quadratic error between the estimated and actual impedance matrices over a set of operating conditions that include all possible combinations of SG commitment statuses. While this method addresses the computational challenges of the analytical approach, it is constrained by the number of SGs in the system, since the number of scenarios grows exponentially with the number of units.

Zhang et al. propose a UC formulation jointly optimized with transmission switching (TS), where SCL are linearized by approximating the impact of SG commitment and line switching on the impedance matrix [49]. Their method derives explicit linear expressions for the change in self-impedance at each bus and embeds minimum SCL limits directly into the UC problem. To mitigate linearization errors —stemming from neglecting mutual impedances— an iterative error-compensation algorithm is introduced, updating the system topology and SG commitment until SCL meet minimum levels. Numerical tests on the IEEE 39- and 300-bus systems show that TS has low impact in the reduction of renewable curtailment when considering minimum SCL constraints.

2.2.2.2 Power system operation models considering SCR-based constraints

Incorporating SCL constraints makes it possible to account for the local nature of system strength. However, the stability issues caused by GFL-IBRs under low system strength conditions can be avoided by reducing their active power output —an aspect that purely SCL-based constraints are unable to capture. Moreover, there are no well-established methodologies for determining appropriate SCL limit values. Consequently, more recent studies have incorporated constraints based on some of the system strength metrics reviewed in section 2.1.2.

Kim et al. recently advanced the integration of system strength criteria into UC by proposing a WSCR-constrained UC model for IBR-dominant power systems [50]. The WSCR captures interactions considering that multiple IBRs in an area are connected to the same busbar. The UC problem is initially formulated as a Mixed-Integer Non-Linear Program (MINLP), since the WSCR depends on the diagonal entries of the bus impedance matrix, which vary with SG commitment. To achieve computational tractability, the authors linearize both the WSCR expression and the bus-impedance modification using McCormick envelopes [48] and the Inverse Matrix Modification Lemma (IMML) [51] resulting in a fully Mixed-Integer Linear Program (MILP) model. The IMML relies on a base-case impedance matrix built from the must-run units committed in a standard UC. Case studies on the IEEE 5-bus, IEEE 39-bus and reduced model of the Korean power system (150 buses, 74 SGs and 76 GFL-IBRs) show that the MILP reformulation successfully increases WSCR levels. However, the WSCR-based formulation assumes that GFL-IBRs inject their nominal power and does not account for electrical distance among these units. As a result, the use of WSCR may lead to overly conservative situations, causing inefficient commitment of SGs.

Wu et al. proposed incorporating the SDSCR into an economic dispatch model, however the relationship between the variables of the model and the SDSCR are highly nonlinear [52]. To embed the SDSCR constraints into the optimization framework, the authors use a multivariate least-squares fitting approach to approximate the nonlinear SDSCR expression as an affine function of the active-power outputs of GFL-IBRs. Case studies on a 109-bus system with six GFL-IBR show that including SDSCR constraints effectively prevents operation in weak-grid conditions. However, commitment decisions of SGs are neglected in this work, which can lead to inefficient dispatch outputs.

A recent line of work by Zhang et al. further expands the modelling scope by jointly considering system-strength constraints and transient overvoltage (TOV) limits within a unified operational framework [53]. The authors develop an optimization model that simultaneously enforces minimum SDSCR requirements and TOV limits derived from time-domain simulations. To overcome the strong nonlinearities associated with both SDSCR and TOV, the method computes trajectory sensitivities of these indices with respect to SGs and GFL-IBRs outputs and linearizes the original nonlinear program into a sequence of linear problems. However, the calculation of the trajectory sensitivities requires continuous time-domain simulations to guard against linearization error, which may be impractical for real-world applications.

Lin et al. develop a UC model that jointly enforces SDSCR, TOV and Transient Voltage Sag (TVS) constraints to prevent wind-turbine tripping in high-wind systems [54]. The original formulation is a large MINLP with differential-algebraic equations (DAEs) and symbolic matrix inversion (admittance matrix). The authors simply device dynamics at critical transient instants to convert the problem into a tractable MINLP. To solve it efficiently they apply generalized Benders decomposition, placing relaxed SDSCR constraints into a MILP master problem (optimizing UC and active power) and the precise SDSCR/TOV/TVS constraints —formulated as Second-Order Cones (SOC) to capture voltage profiles— in NLP subproblems that optimize reactive power and wind-turbines reactive-current gains. Case studies on IEEE-39 bus and IEEE-118 bus show the method accurately predicts voltages at critical moments, mitigates TOV/TVS risks by maintaining strategically located SGs and increases maximum allowable wind capacity. Although the method is efficient for these test systems, it is shown that for a real representation of a power system (50 SGs and 50 wind farms) the model takes several hours to be solved since the approach solves multiple NLP subproblems for each UC iteration.

A different approach incorporated static voltage stability constraints into a UC model [55], employing a SOC relaxation of AC power flow to capture the impact of reactive power on steady-state voltage stability. These constraints are applied to GFL-IBRs and require inversion of the admittance matrix, that depends on decision variables, which the authors address through linearization using a data-driven approach similar to [47]. Similarly, Cui et al. [56] propose a UC framework that optimizes the control mode of IBRs between GFL and GFM to maintain system strength under high renewable penetration. Their formulation includes a system strength constraint based on the gSCR, which models GFM-IBRs as voltage sources that enhance gSCR. Since this metric involves eigenvalue calculations, the authors also adopt a linearized representation using

the data-driven approach from [47]. However, this data-driven method is constrained by the number of SGs in the system, making it impractical for real-world systems with a large number of SG units.

2.2.2.3 Summary

In summary, Table 2.2 presents a comparison of the reviewed works based on the following criteria:

1. Does the model include UC decisions?
2. Does the system strength constraint consider the operating point of GFL-IBRs?
3. Is the system strength constraint used in practice?
4. Is the model scalable for large power systems?
5. Does the work explore the contribution of GFM-IBR?

Table 2.2: Comparison of reviewed works

Ref.	Contribution	Criterion number				
		1.	2.	3.	4.	5.
[45]	Defines SSCFs to linearize SCL constraints. Requires a scaling factor to calibrate the SCL contribution from SGs	✓	X	✓	✓	X
[47]	SCL constraint is linearized using a data-driven approach	✓	X	✓	X	X
[49]	Develops a MILP-based integrated UC&TS. Introduces linear SCL constraints with an error compensation algorithm to mitigate linearization inaccuracies	✓	X	✓	✓	X
[50]	Proposes a WSCR-constrained UC model. The initial MINLP is reformulated into a MILP using McCormick envelopes and the IMML	✓	X	✓	✓	X
[52]	Introduces an economic dispatch model that incorporates SDSCR constraints. These are linearized using a multivariate least-squares fitting approach	X	✓	✓	✓	X
[53]	Develops an UC model that considers SDSCR and TOV constraints. Introduces a linearization approach based on trajectory sensitivities	✓	✓	X	X	X
[54]	Proposes an UC model that considers SDSCR, TOV and TVS constraints. Simplifies the original MINLP with DAEs into an algebraic form and applies generalized Benders decomposition to decompose the problem into a MILP master problem and NLP subproblems	✓	✓	X	X	X
[55]	Proposes a voltage stability-constrained UC model. Derives an analytic criterion for static voltage stability at GFL-IBR buses and reformulates it into SOC form	✓	✓	X	X	X
[56]	Introduces an UC framework that optimizes the control mode of IBRs between GFL and GFM. Minimum gSCR constraint is included which is linearized using a data-driven approach	✓	✓	X	X	✓

Based on the preceding literature survey and the comparison of reviewed works in Table 2.2, this thesis offers several key contributions. First, it proposes a UC model that incorporates system strength constraints grounded in the practically adopted AFL criterion, effectively capturing the operating points of GFL units and the strengthening effects provided by GFM-BESS. Second, it develops and implements an efficient solution algorithm tailored to solve the AFL-constrained UC model for large-scale power systems. Finally, it assesses how battery energy storage systems operating in both GFL and GFM modes influence system strength levels and operational outcomes when such requirements are incorporated.

3 Methodology

This section presents the methodological framework developed to achieve the objectives of this research. It is structured into three main stages: (i) the definition of parameters, variables, and sets required for the optimization model; (ii) the formulation of the UC model incorporating system strength constraints based on the AFL metric; and (iii) the design of a scalable solution strategy based on a cut-generation algorithm to address the computational complexity introduced by these constraints. The proposed methodology combines rigorous mathematical modelling with an algorithmic approach to ensure both accuracy and tractability, enabling its application to realistic large-scale power systems.

3.1 Definition of parameters, variables and sets

The nomenclature of parameters, variables and sets to be used in the optimization model is presented below.

Parameters

$\mathrm{C}_g^{\mathrm{V}}$	Fuel cost, SG g [$/MW]
$\mathrm{C}_g^{\mathrm{SU/SD}}$	Startup/Shutdown cost, SG g [$]
$\mathrm{D}_{d,t}$	Demand, load d, time t [MW]
$\mathrm{E}_b^{\mathrm{min/max}}$	Min./max state of charge, BESS b [MWh]
$\mathrm{E}_b^{0/\mathrm{T}}$	Initial/final state of charge, BESS b [MWh]
$\mathrm{F}_l^{\max}$	Max. power flow, line l [MW]
MSCR_r	Min. short-circuit ratio, renewable generator r
$n^{\max}$	Maximum number of iterations in cut-generation algorithm
$\mathrm{P}_r^{\max}$	Nominal capacity, renewable generator r [MW]
$\mathrm{P}_{r,t}^{\mathrm{av}}$	Available renewable power, renewable generator r, time t [MW]
$\mathrm{P}_b^{\mathrm{dch/ch,max}}$	Max. (dis)charged power, BESS b [MW]
$\mathrm{P}_g^{\mathrm{min/max}}$	Min./max. active power, SG g [MW]
PTDF	Power Transfer Distribution Factors matrix
$\mathrm{P}^{\mathrm{base}}$	Base power [MW]
$\mathrm{R}_g^{\mathrm{U/D}}$	Max. up/down ramping capacity, SG g [MW/h]
$\mathrm{T}_g^{\mathrm{on/off}}$	Min. time on/off, SG g [h]
VoLL	Value of lost load [$/MWh]
X_g''	Subtransient reactance, SG g [p.u.]
X_b''	Subtransient effective reactance, GFM-BESS b [p.u.]
$\mathbf{Y^0}$	Admittance matrix from transmission lines [p.u.]
$\eta_b^{\mathrm{ch/dch}}$	(Dis)charging efficiency, BESS b
Λ_b	Operating mode (1 if operates in GFM mode), BESS b
τ	Violation tolerance in cut-generation algorithm

Variables and functions

$e_{b,t}$	State.of-charge, BESS b, time t [MWh]
$f_{l,t}$	Power flow, line l, time t [MW]
$on_{g,t}$	Startup, SG g, time t

$off_{g,t}$	Shutdown, SG g, time t
$p_{g,t}$	Power output, SG g, time t [MW]
$p_{r,t}$	Power output, renewable generator r, time t [MW]
$p_{b,t}^{\mathrm{dch/ch}}$	(Dis)charging power, BESS b, time t [MW]
$p_{b,t}^{\mathrm{net}}$	Net active power injection, bus i, time t
$u_{g,t}$	Commitment status, SG g, time t
$\boldsymbol{Z}_t^{\mathrm{GFM}}$	Impedance matrix build from GFM units, time t [p.u.]
$\boldsymbol{Z}_t^{\mathrm{proxy}}$	Impedance matrix considering GFL units, time t [p.u.]
$\mu_{b,t}$	State of operation, BESS b, time t
Indices and sets	
$b, \tilde{b} \in B, B_i$	BESS in the system, in bus i
$d, \tilde{d} \in D, D_i$	Loads in the system, in bus i
$g, \tilde{g} \in G, G_i$	SGs in the system, in bus i
$i \in N$	Buses in the system
$l \in L$	Lines in the system
n	Iteration number in cut-generation algorithm
$r, \tilde{r} \in R, R_i$	Renewable generators in the system, in bus i
$t \in T$	Hours in time window

3.2 Development of AFL-constrained UC model

3.2.1 Model overview

The proposed AFL-constrained UC model aims to determine, for each hour in the day-ahead horizon, the optimal commitment and dispatch of SGs, the active power output of IBRs operating in GFL mode, and the operation of BESS, which may operate either in GFL or GFM mode. These decisions are co-optimized to minimize the total operating cost while ensuring adequate system strength, expressed through the AFL requirement at the buses of the system.

The model assumes a DC power flow representation using Power Transfer Distribution Factors (PTDFs) for active power balance and flow through transmission lines, with a fixed network topology throughout the horizon. SGs and BESS operating in GFM mode are treated as voltage sources that contribute to SCL, whereas GFL units do not provide fault current. The AFL metric is enforced by ensuring that the SCL provided by voltage sources is sufficient to offset the SCL "consumed" by GFL units, which is calculated based on their active power output rather than nominal capacity.

The model takes as input hourly demand and renewable availability profiles, SGs techno-economic data such as minimum and maximum outputs, ramp rates, minimum on/off times, fuel costs, and startup/shutdown costs. It also incorporates BESS parameters including energy capacity, charging and discharging power limits, and state-of-charge (SoC) bounds, as well as network data such as the PTDF matrix and line power flow limits. System strength data include SG subtransient reactances, effective subtransient reactances for GFM-BESS, and minimum short-circuit ratio (MSCR) requirements for renewable GFL units.

The decision variables include the on/off status of SGs, hourly active power dispatch of SGs and renewable units, BESS charge and discharge power, and SoC. Load shedding is allowed and penalized through a value of lost load (VoLL). The objective function minimizes the total operating cost, which comprises fuel costs, startup and shutdown costs, and penalties for any load shedding.

The model enforces several categories of constraints. These include power balance and transmission limits, thermal unit operational constraints such as ramping and minimum on/off times, renewable generation limits based on resource availability, and BESS operational constraints related to charging, discharging, and energy balance. Most importantly, system strength is enforced through AFL constraints. AFL is computed by comparing two network views. In the first one, the impedance matrix is built from only considering SGs and GFM-BESS as voltage sources. In the second one, GFL units are also modelled as equivalent voltage sources behind an impedance, which is sized according to their MSCR and active power output. This approach captures the local nature of system strength and its dependency on operating conditions.

Because the AFL constraint introduces strong nonlinearities into the UC problem, the exact formulation results in a MINLP that is computationally prohibitive to solve for large-scale systems. To overcome this challenge, the model employs an iterative cut-generation algorithm that replaces the original nonlinear constraint with a sequence of linear outer approximations. At each iteration, cuts are generated from eigenvectors associated with violations of matrix inequalities, progressively tightening the feasible region until no AFL violations remain. This strategy transforms the problem into a sequence of MILPs enabling scalability and practical applicability.

The outputs of the model include a feasible UC schedule, hourly dispatch of all resources, renewable curtailment levels, operating costs, and AFL profiles across the buses of the system. By internalizing system strength constraints into the UC, the proposed model provides a cost-efficient and secure operational strategy that maintains adequate system strength levels in systems with deep IBR-penetration.

3.2.2 Objective function

The objective function shown in (3.1), minimises the system's total operational costs. These include the fuel costs of SGs, startup and shutdown, and VoLL.

$$\min_{p_{g,t},on_{g,t},off_{g,t},ls_{d,t}} \sum_{t\in T}\left[\sum_{g\in G}\left(\mathrm{C}_g^{\mathrm{V}}p_{g,t}+\mathrm{C}_g^{\mathrm{SU}}on_{g,t}+\mathrm{C}_g^{\mathrm{SD}}off_{g,t}\right)+\sum_{d\in D}\left(\mathrm{VoLL}\cdot ls_{d,t}\right)\right] \tag{3.1}$$

3.2.3 Transmission constraints and balance equation

For this work, active power flows in lines are calculated based on the PTDF matrix (see Annex A). This formulation allows the active power flows in lines to be expressed as a linear function of the net power injections at the buses of the system, eliminating the phase angle variables and simplifying the model [57]. Then, the active power flow on a transmission line can be calculated as in (3.2) and the forward and reverse maximum capacity of lines are modelled as presented in (3.3).

$$f_{l,t} = \sum_{i \in N} [\mathbf{PTDF}]_{l,i} p_{i,t}^{\text{net}} \qquad \forall l \in L, \forall t \in T \quad (3.2)$$

$$-\mathrm{F}_l^{\max} \leq f_{l,t} \leq \mathrm{F}_l^{\max} \qquad \forall l \in L, \forall t \in T \quad (3.3)$$

Equation (3.4) shows that the net power injection is calculated as the difference between the injected and the consumed active power in every bus i at every hour t. Then, the global balance constraint in (3.5) ensures that the sum of active power from all nodal injections and consumptions is zero.

$$p_{i,t}^{\text{net}} = \sum_{\tilde{g} \in G_i} p_{\tilde{g},t} + \sum_{\tilde{r} \in R_i} p_{\tilde{r},t} + \sum_{\tilde{b} \in B_i} \left(p_{\tilde{b},t}^{\text{dch}} - p_{\tilde{b},t}^{\text{ch}}\right) - \sum_{\tilde{d} \in D_i} \left(\mathrm{D}_{\tilde{d},t} - ls_{\tilde{d},t}\right) \qquad \forall i \in N, \forall t \in T \quad (3.4)$$

$$\sum_{i \in N} p_{i,t}^{\text{net}} = 0 \qquad \forall t \in T \quad (3.5)$$

3.2.4 SG constraints

The SG constraints model the scheduling and commitment of SG units, ramp limitations, startup, shutdown and minimum on-off times. These constraints are given by (3.6)-(3.14). The startup and shutdown transitions are described by (3.6) and (3.7). The minimum up-times and down-times are modelled through (3.8)-(3.9) and (3.10)-(3.11), respectively. The maximum and minimum power output of SGs is given by (3.12). SGs have a maximum ramp rate limit. These constraints are shown in (3.13) and (3.14).

$$on_{g,t} - off_{g,t} = u_{g,t} - u_{g,t-1} \qquad \forall g \in G, \forall t \in [2, T] \quad (3.6)$$

$$on_{g,t} + off_{g,t} \leq 1 \qquad \forall g \in G, \forall t \in T \quad (3.7)$$

$$u_{g,t} \geq \sum_{\tilde{t}=1}^{t} on_{g,\tilde{t}} \qquad \forall g \in G, \forall t \in [1, \mathrm{T}_g^{\text{on}}] \quad (3.8)$$

$$u_{g,t} \geq \sum_{\tilde{t}=t-\mathrm{T}_g^{on}}^{t} on_{g,\tilde{t}} \qquad \forall g \in G, \forall t \in [1 + \mathrm{T}_g^{\text{on}}, T] \quad (3.9)$$

$$u_{g,t} \leq 1 - \sum_{\tilde{t}=1}^{t} off_{g,\tilde{t}} \qquad \forall g \in G, \forall t \in [1, \mathrm{T}_g^{\text{off}}] \quad (3.10)$$

$$u_{g,t} \leq 1 - \sum_{\tilde{t}=t-\mathrm{T}_g^{off}}^{t} off_{g,\tilde{t}} \qquad \forall g \in G, \forall t \in [1 + \mathrm{T}_g^{\text{off}}, T] \quad (3.11)$$

$$\mathrm{P}_g^{\min} u_{g,t} \leq p_{g,t} \leq \mathrm{P}_g^{\max} u_{g,t} \qquad \forall g \in G, \forall t \in T \quad (3.12)$$

$$p_{g,t} - p_{g,t-1} \leq R_g^{\mathrm{U}} u_{g,t-1} + R_g^{\mathrm{U}} on_{g,t} \qquad \forall g \in G, \forall t \in [2,T] \quad (3.13)$$

$$p_{g,t-1} - p_{g,t} \leq R_g^{\mathrm{D}} u_{g,t-1} + R_g^{\mathrm{D}} off_{g,t} \qquad \forall g \in G, \forall t \in [2,T] \quad (3.14)$$

3.2.5 Renewable generation constraints

The renewable output is constrained in (3.15) by the availability of wind and solar resource in period t.

$$p_{r,t} \leq \mathrm{P}_{r,t}^{\mathrm{av}} \qquad \forall r \in R, \forall t \in T \quad (3.15)$$

3.2.6 BESS constraints

The operation of BESS is modelled in equations (3.16)-(3.21). Binary variable $\mu_{b,t}$ is employed to determine if BESS b is in charging $(\mu_{b,t} = 0)$ or discharging mode $(\mu_{b,t} = 1)$. Equations (3.16) and (3.17) limit the charging and discharging power depending on the available maximum capacity for each unit. The energy balance of BESS is described in (3.18)-(3.21).

$$p_{b,t}^{\mathrm{ch}} \leq (1 - \mu_{b,t}) \mathrm{P}_b^{\mathrm{ch,max}} \qquad \forall b \in B, \forall t \in T \quad (3.16)$$

$$p_{b,t}^{\mathrm{dch}} \leq \mu_{b,t} \mathrm{P}_b^{\mathrm{dch,max}} \qquad \forall b \in B, \forall t \in T \quad (3.17)$$

$$e_{b,t} = \eta_b^{\mathrm{ch}} p_{b,t}^{\mathrm{ch}} - \frac{p_{b,t}^{\mathrm{dch}}}{\eta_b^{\mathrm{dch}}} + e_{b,t-1} \qquad \forall b \in B, \forall t \in [2,T] \quad (3.18)$$

$$\mathrm{E}_b^{\mathrm{min}} \leq e_{b,t} \leq \mathrm{E}_b^{\mathrm{max}} \qquad \forall b \in B, \forall t \in T \quad (3.19)$$

$$e_{e,0} = \mathrm{E}^0 \qquad \forall b \in B \quad (3.20)$$

$$e_{e,\mathrm{T}} = \mathrm{E}^{\mathrm{T}} \qquad \forall b \in B \quad (3.21)$$

3.2.7 AFL constraints

The AFL quantifies the impact of GFL units at any busbar in the system. The presence of a connected GFL unit is modelled as an equivalent reduction in the SCL provided by GFM units (SGs and GFM-BESS). Specifically, the reduction in SCL at the PoC of a GFL unit is assumed, initially, to be equal to its nominal capacity multiplied by its MSCR, which represents the lowest SCR value required at the PoC to ensure code-compliant performance. To estimate the impact of a GFL unit located deeper within the network, the superposition principle is employed. In the first step, the reduction in SCL caused by the GFL is represented as an equivalent "increase" in fault level at the same point, by modelling the GFL unit as a voltage source behind an effective impedance— defined in (3.22).

$$\mathrm{Y}_r^{\mathrm{GFL}} = \frac{\mathrm{MSCR}_r \mathrm{P}_r^{\max}}{\mathrm{P}^{\mathrm{base}}} \qquad \forall r \in R \quad (3.22)$$

However, renewable generators typically do not operate at their maximum rated capacity. As a result, when the SCL reduction by GFL units is calculated using nominal values —as in (3.22)— it may be overestimated. This can lead to excessive requirements of SCL provided from committed SGs and GFM-BESS. To address this, (3.22) is reformulated to account for the operational active power injection of GFL-IBRs, yielding (3.23).

$$y_{r,t}^{\mathrm{GFL}} = \frac{\mathrm{MSCR}_r p_{r,t}}{\mathrm{P}^{\mathrm{base}}} \qquad \forall r \in R, t \in T \quad (3.23)$$

Using superposition, this equivalent increase in SCL at any bus reflects the potential reduction in SCL due to the presence of the GFL unit. Consequently, the AFL at a given bus is defined as the "remaining" SCL after subtracting the "consumed" SCL attributed to connected GFL units. Then, to ensure grid code compliance of GFL units across the system, the minimum AFL requirement at the buses of interest is zero. Following the calculation procedure outlined in [39], it can be demonstrated that the AFL at a bus i and time t can be computed as (3.24).

$$\mathrm{AFL}_{i,t} = 2SCL_{i,t}^{\mathrm{GFM}} - SCL_{i,t}^{\mathrm{proxy}} \geq 0 \qquad \forall i \in N, \forall t \in T \quad (3.24)$$

Where $SCL_{i,t}^{\mathrm{GFM}}$ denotes the SCL at bus i, time t provided by all operational GFM units (including committed SGs and GFM-BESS) in the system. $SCL_{i,t}^{\mathrm{proxy}}$ represents the SCL at bus i, time t when GFL units are modelled as voltage sources behind their effective impedance, which can be calculated as described in (3.23). From (3.24), it is worth noting that when no GFL units are present in the system, the AFL reduces to the traditional SCL.

The AFL can be expressed in terms of the equivalent impedance seen from each bus in the system. By assuming nominal voltages in per-unit and neglecting system resistances, (3.24) can be reformulated as (3.25).

$$\left[\boldsymbol{Z}_t^{\mathrm{GFM}}\right]_{i,i} \leq 2\left[\boldsymbol{Z}_t^{\mathrm{proxy}}\right]_{i.i} \qquad \forall i \in N, \forall t \in T \quad (3.25)$$

Where $\left[\boldsymbol{Z}_t^{\mathrm{GFM}}\right]_{i,i}$ and $\left[\boldsymbol{Z}_t^{\mathrm{proxy}}\right]_{i,i}$ correspond to the ith diagonal elements of the impedance matrices computed by modelling only GFM units as voltage sources ($\boldsymbol{Z}_t^{\mathrm{GFM}}$), and by additionally representing the GFL units as voltage sources ($\boldsymbol{Z}_t^{\mathrm{proxy}}$), respectively. The Z-matrices must meet (3.26) and (3.27).

$$\boldsymbol{Z}_t^{\mathrm{GFM}} \cdot \boldsymbol{Y}_t^{\mathrm{GFM}} = \mathbf{I_N} \qquad \forall t \in T \quad (3.26)$$

$$\boldsymbol{Z}_t^{\mathrm{proxy}} \cdot \boldsymbol{Y}_t^{\mathrm{proxy}} = \mathbf{I_N} \qquad \forall t \in T \quad (3.27)$$

Where $\mathbf{I_N}$ is the N-dimensional identity matrix. Equations (3.26) and (3.27) can be rewritten as (3.28) and (3.29), respectively.

$$\sum_{k\in N}\left[\boldsymbol{Z}_t^{\mathrm{GFM}}\right]_{k,j}\left(\left[\mathbf{Y}^0\right]_{i,i}+y_{i,t}^{\mathrm{GFM}}\right)=\begin{cases}1, & i=j\\ 0, & i\neq j\end{cases} \qquad \forall i,j\in N,\forall t\in T \quad (3.28)$$

$$\sum_{k\in N}\left[\boldsymbol{Z}_t^{\mathrm{proxy}}\right]_{k,j}\left(\left[\mathbf{Y}^0\right]_{i,i}+y_{i,t}^{\mathrm{GFM}}+y_{i,t}^{\mathrm{GFL}}\right)=\begin{cases}1, & i=j\\ 0, & i\neq j\end{cases} \qquad \forall i,j\in N,\forall t\in T \quad (3.29)$$

Where $y_{i,t}^{\mathrm{GFM}}$ contains the subtransient admittance of the SGs, which depend on their commitment status, as described in (3.30), as well as the effective admittance of GFM-BESS, as again described in (3.30) (BESS units do not need to be committed, but they need to be operating in GFM mode denoted by $\Lambda_b = 1$). Similarly, $y_{i,t}^{\mathrm{GFL}}$ is determined by the active power output from GFL units, as in (3.31).

$$y_{i,t}^{\mathrm{GFM}}=\sum_{\tilde{g}\in G_i}\frac{1}{\mathrm{X}_{\tilde{g}}''}u_{\tilde{g},t}+\sum_{\tilde{b}\in B_i}\frac{1}{\mathrm{X}_{\tilde{b}}''}\Lambda_{\tilde{b}} \qquad \forall i\in N,\forall t\in T \quad (3.30)$$

$$y_{i,t}^{\mathrm{GFL}}=\sum_{\tilde{r}\in R_i}\frac{\mathrm{MSCR}_{\tilde{r}}p_{\tilde{r},t}}{\mathrm{P^{base}}} \qquad \forall i\in N,\forall t\in T \quad (3.31)$$

By replacing (3.30) and (3.31) into (3.28) and (3.29), and treating each element of $\boldsymbol{Z}_t^{\mathrm{GFM}}$ and $\boldsymbol{Z}_t^{\mathrm{proxy}}$ as decision variables, nonlinearities arise from the product of continuous decision variables (i.e., $\left[\boldsymbol{Z}_t^{\mathrm{GFM}}\right]_{k,j}$ and $\left[\boldsymbol{Z}_t^{\mathrm{proxy}}\right]_{k,j}$) with binary decision variables (commitment of SGs) and with continuous decision variables (active power injection of renewable GFLs). Then, incorporating (3.26) and (3.27) to the UC, involve the addition of $2\mathrm{N}^2$ equality constraints with multiplication of decision variables. Then the UC model with AFL constraints is a MINLP, which is prohibitive to solve in large-scale power systems.

3.3 Development of solution algorithm

To address the scalability of the problem of the MINLP AFL-constrained UC model, the original problem is relaxed through a linear approximation framework, in which linear cuts are iteratively generated. Considering the condition in (3.32), then (3.25) can be reformulated as (3.33).

$$\boldsymbol{Z}_t^{\mathrm{GFM}}=\left[\boldsymbol{Y}_t^{\mathrm{GFM}}\right]^{-1} \qquad \forall t\in T \quad (3.32)$$

$$\left[\boldsymbol{Y}_t^{\mathrm{GFM}}\right]_{i,i}^{-1}\leq 2\left[\mathbf{Z}_t^{\mathrm{proxy}}\right]_{i,i} \qquad \forall i\in N,\forall t\in T \quad (3.33)$$

Since $\boldsymbol{Y}_t^{\mathbf{GFM}}$ is symmetric and positive definite (see Annex B), is invertible and, in particular, (3.34) holds.

$$\left[\boldsymbol{Y}_t^{\mathrm{GFM}}\right]_{i,i}^{-1}=e_i^{\mathrm{T}}\cdot\left[\boldsymbol{Y}_t^{\mathrm{GFM}}\right]^{-1}\cdot e_i \qquad \forall i\in N,\forall t\in T \quad (3.34)$$

Where e_i is the ith canonical vector. Then, (3.32) can be rewritten as (3.35).

$$2\left[\mathbf{Z}_t^{\mathrm{proxy}}\right]_{i,i}-e_i^{\mathrm{T}}\cdot\left[\boldsymbol{Y}_t^{\mathrm{GFM}}\right]^{-1}\cdot e_i\geq 0 \qquad \forall i\in N,\forall t\in T \quad (3.35)$$

By Schur complement [58], inequality (3.35) can be equivalently expressed as the Linear Matrix Inequality (LMI) [59] shown in (3.36).

$$\boldsymbol{M}_{i,t} = \begin{bmatrix} \boldsymbol{Y}_t^{\mathrm{GFM}} & e_i \\ e_i^{\mathrm{T}} & 2\left[\mathbf{Z}_t^{\mathrm{proxy}}\right]_{i,i} \end{bmatrix} \succcurlyeq 0 \qquad \forall i \in N, \forall t \in T \quad (3.36)$$

Adding constraint (3.36) to the model results in a Semi-Definite Program (SDP). Solving via SDP solvers may be computationally prohibitive for large-scale systems, due to both time and memory requirements. Moreover, SDP constraints are often incompatible with mixed-integer formulations. However, the feasible set defined by (3.36) can be approximated through a set of linear outer approximations. Indeed, (3.36) must be met for any test vector $\mathbf{v}$ and scalar α, then the constraint can be restated as the infinite family of inequalities shown in (3.37).

$$\begin{bmatrix} \mathbf{v} \\ \alpha \end{bmatrix}^{\mathrm{T}} \cdot \boldsymbol{M}_{i,t} \cdot \begin{bmatrix} \mathbf{v} \\ \alpha \end{bmatrix} \geq 0 \qquad \forall i \in N, \forall t \in T, \forall \mathbf{v} \in \mathbb{R}^{\mathrm{N}}, \forall \alpha \in \mathbb{R} \quad (3.37)$$

Specifically, consider the vector $\mathbf{x}$ given by $\mathbf{x} \coloneqq \begin{bmatrix} \mathbf{v} \\ -\mathrm{v}_i \big/ 2\left[\mathbf{Z}_t^{\mathrm{proxy}}\right]_{i,i} \end{bmatrix}$. Substituting $\mathbf{x}$ in (3.37) yields (3.38).

$$\mathbf{x}^{\mathrm{T}} \cdot \boldsymbol{M}_{i,t} \cdot \mathbf{x} \geq 0 \qquad \forall i \in N, \forall t \in T \quad (3.38)$$

Expanding (3.38) yields (3.39).

$$\mathbf{x}^{\mathrm{T}} \cdot \boldsymbol{M}_{i,t} \cdot \mathbf{x} = \mathbf{v}^{\mathrm{T}} \cdot \boldsymbol{Y}_t^{\mathrm{GFM}} \cdot \mathbf{v} - \frac{\mathrm{v}_i^2}{2\left[\mathbf{Z}_t^{\mathrm{proxy}}\right]_{i,i}} \qquad \forall i \in N, \forall t \in T, \forall \mathbf{v} \in \mathbb{R}^{\mathrm{N}} \quad (3.39)$$

Then, substituting (3.39) in (3.38) yields (3.40).

$$\mathbf{v}^{\mathrm{T}} \cdot \boldsymbol{Y}_t^{\mathrm{GFM}} \cdot \mathbf{v} \geq \frac{\mathrm{v}_i^2}{2\left[\mathbf{Z}_t^{\mathrm{proxy}}\right]_{i,i}} \qquad \forall i \in N, \forall t \in T, \forall \mathbf{v} \in \mathbb{R}^{\mathrm{N}} \quad (3.40)$$

Since (3.40) must hold for all test vectors $\mathbf{v}$, the feasible region remains convex but is not directly tractable. To obtain linear constraints, the matrix form can be decomposed into diagonal and off-diagonal components as in (3.41).

$$\mathbf{v}^{\mathbf{T}} \cdot \boldsymbol{Y}_t^{\mathrm{GFM}} \cdot \mathbf{v} = \sum_{j \in N} \mathrm{v}_j^2 \left[\boldsymbol{Y}_t^{\mathrm{GFM}}\right]_{j,j} + 2 \sum_{j,j' \in N, j \neq j'} \left[\boldsymbol{Y}_t^{\mathrm{GFM}}\right]_{j,j'} \mathrm{v}_j \mathrm{v}_{j'} \qquad \forall t \in T, \forall \mathbf{v} \in \mathbb{R}^{\mathrm{N}} \quad (3.41)$$

Notice that $\left[\boldsymbol{Y}_t^{\mathrm{GFM}}\right]_{j,j'}$ are parameters in $\boldsymbol{Y}_t^{\mathrm{GFM}}$ (decision variables are only in the diagonal). Substituting (3.41) into (3.40) yields linear inequalities in the diagonal entries of $\boldsymbol{Y}_t^{\mathrm{GFM}}$ as in (3.42).

$$\sum_{j \in N} \mathrm{v}_j^2 \left[\boldsymbol{Y}_t^{\mathrm{GFM}}\right]_{j,j} \geq \frac{\mathrm{v}_i^2}{2\left[\mathbf{Z}_t^{\mathrm{proxy}}\right]_{i,i}} - 2 \sum_{j,j' \in N, j \neq j'} \left[\boldsymbol{Y}_t^{\mathrm{GFM}}\right]_{j,j'} \mathrm{v}_j \mathrm{v}_{j'}$$

$$\forall i \in N, \forall t \in T, \forall \mathbf{v} \in \mathbb{R}^{\mathrm{N}} \quad (3.42)$$

Since the set of valid inequalities (3.42) is infinite, it is proposed the cut-generation algorithm shown in Figure 3.1. The core idea behind this algorithm is to identify if there exists a vector $\mathbf{v}$ that follows (3.43).

$$\mathbf{v}^{\mathrm{T}} \cdot \boldsymbol{M}'_{i,t} \cdot \mathbf{v} < -\tau \qquad \forall i \in N, \forall t \in T, \forall \mathbf{v} \in \mathbb{R}^{\mathrm{N}} \quad (3.43)$$

Where τ is a small positive number and $\boldsymbol{M}'_{i,t}$ is defined as in (3.44):

$$\boldsymbol{M}'_{i,t} \coloneqq \boldsymbol{Y}_t^{\mathrm{GFM}} - \frac{1}{2\left[\mathbf{Z}_t^{\mathrm{proxy}}\right]_{i,i}} e_i e_i^{\mathrm{T}} \qquad \forall i \in N, \forall t \in T \quad (3.44)$$

If a vector **v** meets (3.43), then (3.36) is violated (matrix $\boldsymbol{M}_{i,t}$ is not semidefinite positive). Therefore, vector **v** serves as an effective cutting direction, as it yields the linear inequality in (3.42). The most suitable choice for **v** to detect such violations is the eigenvector associated to the smallest eigenvalue of $\boldsymbol{M}'_{i,t}$ which represents the direction of greatest violation. Then, the UC is solved iteratively considering the set of linear inequalities from eigenvectors **v** that meet (3.43) in the previous iteration. The algorithm stops if there are no vectors that meet (3.43) or if the maximum number of iterations is reached (denoted as $n^{\max}$ in Figure 3.1). Through the cut-generation algorithm, the LMI (3.36) is replaced by a sequence of MILP problems, significantly reducing computational burden.

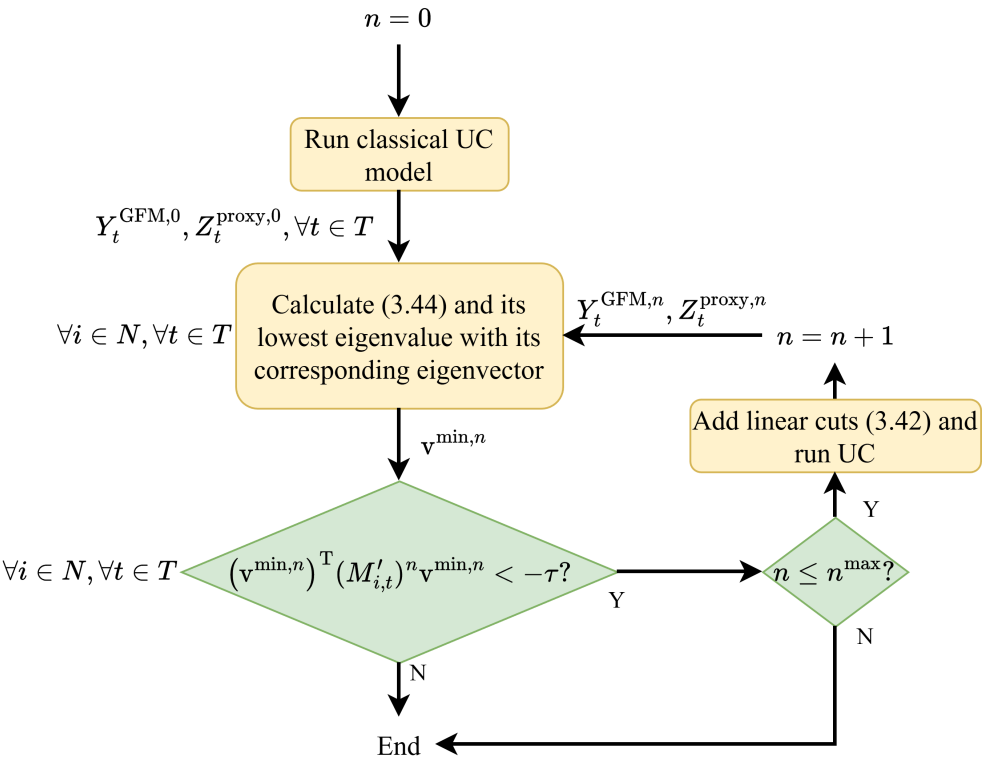


Figure 3.1: Diagram of cut-generation algorithm. n denotes the iteration number.

4 Results and analysis

This section presents and analyses the results obtained by applying the AFL-constrained UC model proposed in Section 3.2 and solved with the cut-generation algorithm proposed in Section 3.3. This chapter also describes the system model and the scenarios employed in this work. The input data presented in this section use as their main source the information presented in [60] and [61]. The analysis focuses on evaluating the performance of the proposed model in meeting adequate system strength levels, the operational impact of incorporating system strength constraints, and the role of BESS under different operating modes. Comparative assessments are provided against the classical UC formulation to quantify the techno-economic implications of enforcing minimum AFL requirements. Additionally, sensitivity analyses explore the influence of enabling AFL-driven curtailment and contrast the proposed approach with typical security-constraints imposed by system operators. Future system scenarios are examined to assess the operational value that can be unlocked with the proposed methodology, specifically, under increasing renewable penetration and coal phase-out conditions. Finally, the performance of the cut-generation algorithm is analysed.

4.1 System characterization and input data

Case study applications are based on a realistic representation of the Chilean Power System (CPS) presented in Figure 4.1(a). The Chilean power system is characterized as an isolated and weakly meshed network, resulting in low levels of system strength. According to Figure 4.1(b), the Great North (NG by the acronym in Spanish) of Chile has a high availability of solar resources,

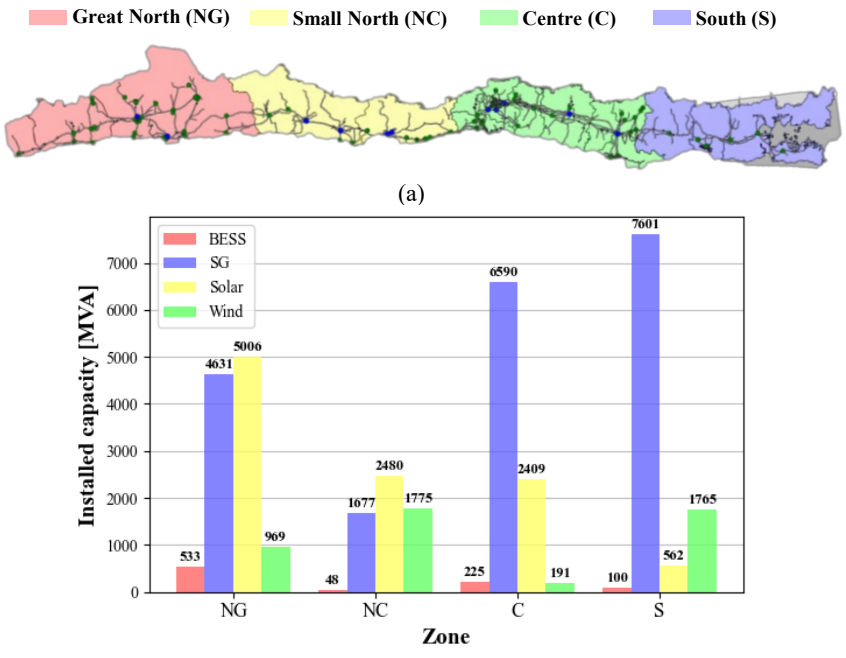


Figure 4.1: (a) Map of the CPS. (b) Installed capacity in the CPS by region and technology.

leading to a significant penetration of IBRs in that region. Moreover, since the CPS is not interconnected with its neighbouring countries and its synchronous generation capacity resides primarily in the Centre and South, the NG region is characterized by having low system strength levels. Therefore, case study applications are focused on this region of the CPS. The graph representing the NG region of the CPS is shown in Figure 4.2. For all GFL-IBRs, a MSCR of 1.8

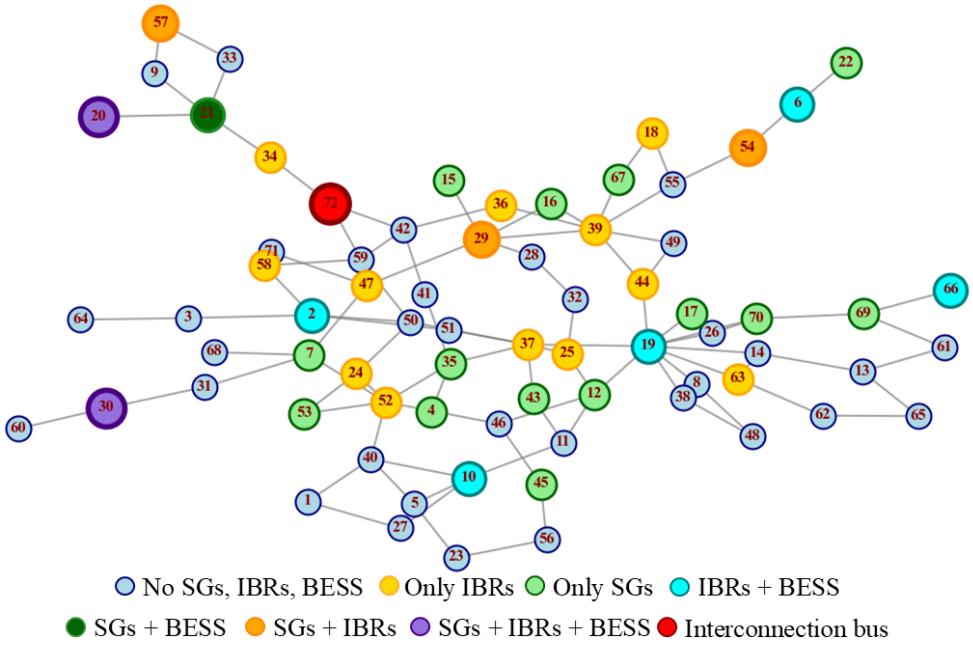


Figure 4.2: Graph representation of the NG region.

is assumed, which aligns with the standard value recommended by AEMO [40]. Finally, the VoLL is set at 10,400 $/MWh. Techno-economic parameters of SGs and BESS can be found in Appendix C.

For the case study, a day characterized by low demand and high renewable penetration is selected, as this scenario represents a worst-case condition from the perspective of system strength due to the reduced number of committed SGs. The renewable generation and demand profiles are shown in Figure 4.3, where the high availability of solar resources throughout daylight hours is evident, with solar output even exceeding demand during portions of the day. This operating condition creates a challenging scenario for maintaining adequate system strength, since the displacement of synchronous generation by renewable energy sources typically leads to lower SCL. Consequently, such a day provides a suitable benchmark for evaluating the effectiveness of the proposed UC model and for assessing how the inclusion of system strength requirements influences scheduling decisions, renewable curtailment, and the role of BESS in both GFL and GFM modes.

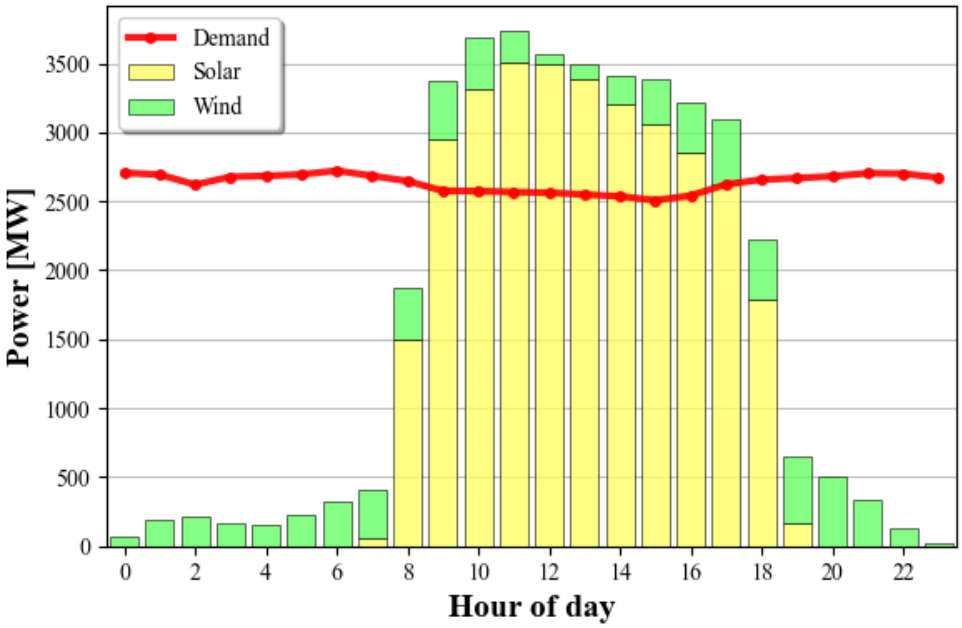
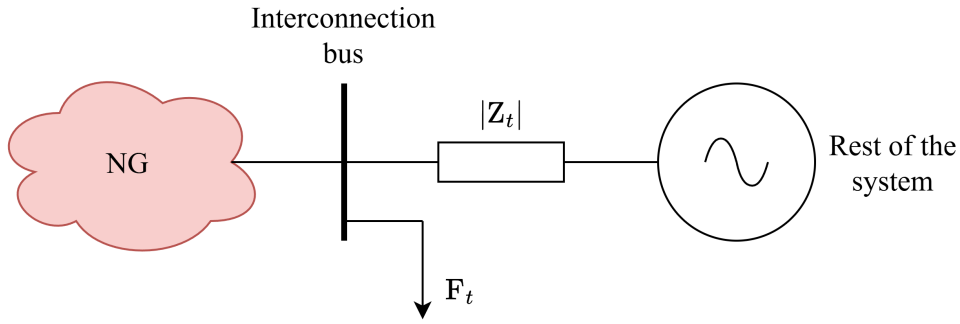


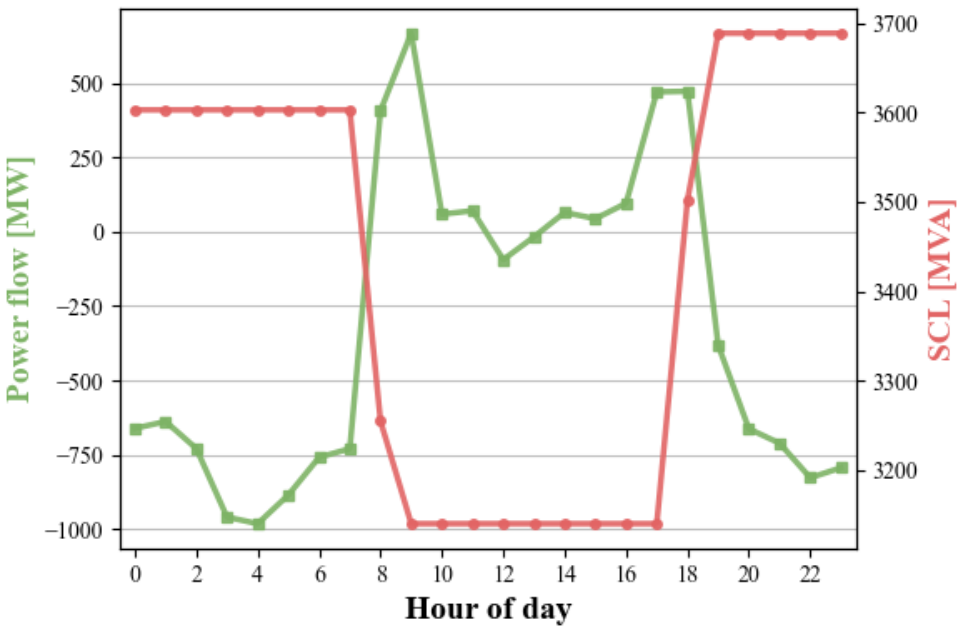
Figure 4.3: Renewable and demand profiles for NG region in the CPS.

The contribution of the rest of the CPS is represented by an equivalent voltage source and an equivalent demand at the interconnection bus (bus 72 in Figure 4.2), as illustrated in Figure 4.4(a). The equivalent voltage source provides short-circuit power to the NG region, which varies depending on the commitment of synchronous units in the rest of the system. Similarly, the equivalent demand reflects the power exchange between the NG region and the rest of the system, which also changes on an hourly basis. To obtain these SCL and power flow profiles, a classical UC is performed for the entire CPS. For the selected day, the resulting SCL and power flow profiles are presented Figure 4.4(b).

The power flow profile shown in Figure 4.4(b) reveals an import of active power from the rest of the system to the NG region during nighttime hours (negative values indicate import, while positive values indicate export). Conversely, daylight hours are predominantly characterized by power export from the NG region. Notably, export peaks occur in the morning (08:00–09:00) and late afternoon (17:00–18:00), coinciding with peak demand periods in the CPS. On the other hand, the SCL profile shows a higher SCL contribution from the rest of the CPS to the NG region during nighttime hours, and a lower contribution during daylight hours. This pattern reflects the number of SG units committed in the CPS. Due to the system's high solar availability, fewer SGs are committed during the day, resulting in a lower overall SCL. Conversely, at night, when solar generation is absent, more SGs are committed to meet demand, leading to a higher SCL contribution.



(a)



(b)

Figure 4.4: (a) Representation of the rest of the CPS. (b) Power flow and SCL profiles at the interconnection bus between the NG region and the rest of the system.

4.2 Performance of the proposed model

This section evaluates the model's ability to satisfy AFL requirements through six case studies: (i) without BESS in the NG region, (ii) with BESS operating in GFL mode, and (iii) with BESS operating in GFM mod, each solved using both the classical UC model and the proposed AFL-constrained UC model. The UC model and cut-generation algorithm were implemented in Julia using JuMP [62] and solved with Gurobi 12.0.0 [63], imposing a maximum tolerance for the MIP gap of 0.01%. Simulations were performed on a computer equipped with an AMD Ryzen 5 5500 U processor and 8 GB of RAM.

Figure 4.5 presents the minimum AFL across the system for each hour of the day for all case studies. When AFL constraints are not enforced, significant violations occur during daylight hours due to the dominance of solar generation in the NG region. The most severe shortfalls appear in the BESS-GFL case because fewer SGs are committed compared to the scenario without BESS,

as these units provide a more cost-effective solution for balancing the system. However, BESS in

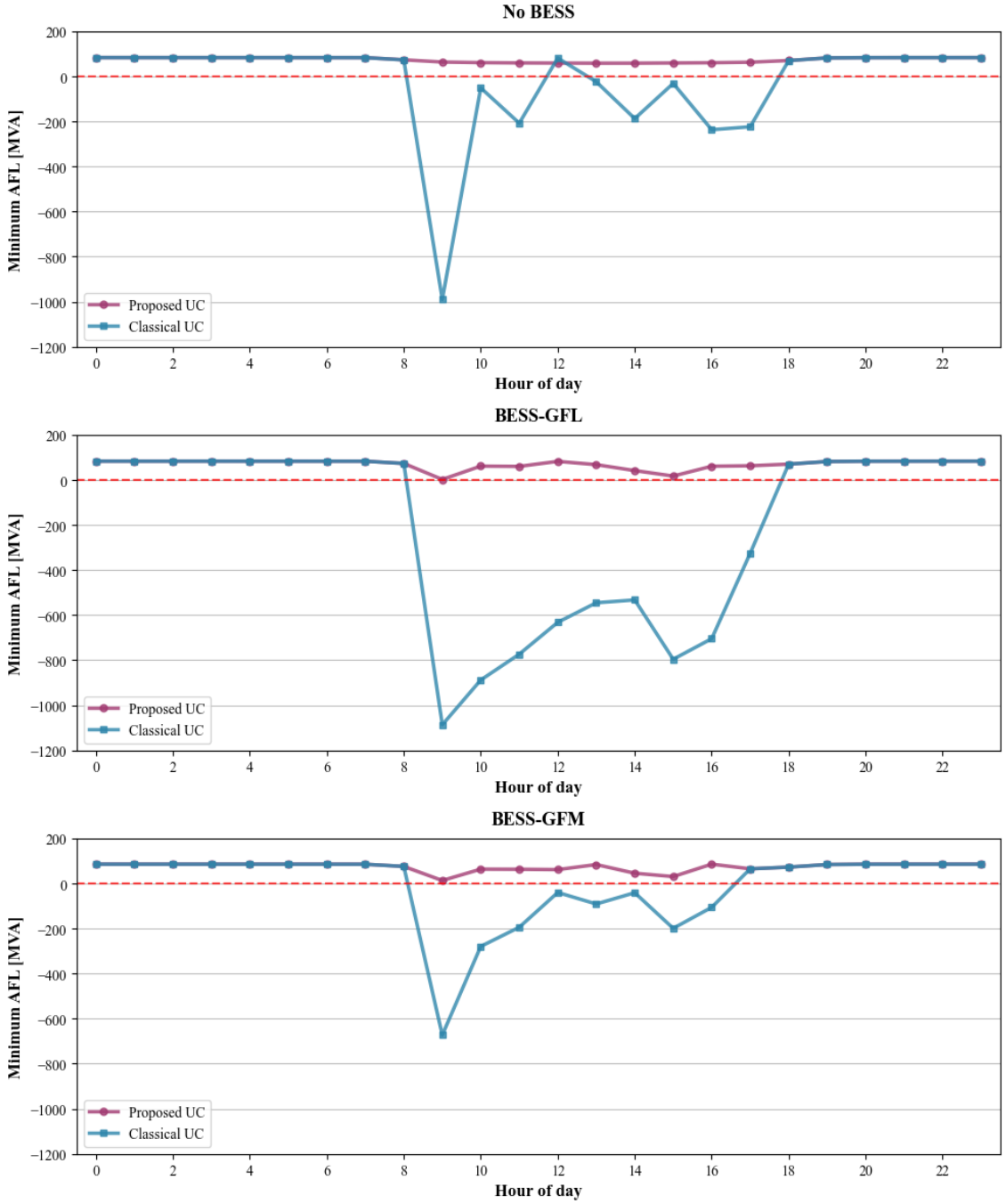


Figure 4.5: Minimum AFL in the NG region throughout the day with classical and proposed UC models.

GFL mode does not contribute to SCL, whereas BESS in GFM mode strengthens the grid by providing SCL, thereby reducing AFL shortfalls.

Figure 4.5 also shows that, under the proposed model, AFL remains positive throughout the day, always ensuring adequate system strength levels. In the scenario without BESS, the minimum

AFL during daylight hours remains relatively stable at around 100 MVA, whereas in the BESS-GFL and BESS-GFM cases, the minimum AFL fluctuates significantly and even drops close to zero at certain hours. This difference arises because, without BESS, additional SGs must be committed to supply SCL. These units operate at their minimum stable output, which increases renewable curtailment and, consequently, raises AFL levels. In contrast, the presence of BESS enhances system flexibility, reducing renewable curtailment and thereby making the AFL profiles more variable across the day.

4.3 Analysis on system operation

This section investigates the impact of including AFL requirements on system operation. The daily operating cost and renewable curtailment are summarized in Table 4.1 and Table 4.2, respectively. Compared to the classical UC model, incorporating the minimum AFL requirement results in daily operating costs increases of 2.9%, 8.1% and 5.4% for the scenarios without BESS, with BESS-GFL and with BESS-GFM, respectively. Similarly, daily renewable curtailment rises by 10.6%, 24.9% and 13.3% across the same cases. These results highlight that, to satisfy the minimum AFL requirement, the model tends to commit additional SGs to provide SCL. The most pronounced difference occurs in the BESS-GFL case, where AFL levels are significantly lower than in the other scenarios according to Figure 4.5. To compensate for these shortfalls, additional SGs must be committed, leading to increased daily operating costs.

Table 4.1: Daily operating cost with classical and proposed UC model.

	Classical UC [k$]	**Proposed UC** [k$]	**Difference** [%]
No BESS	947.7	975.2	2.9
BESS-GFL	762.3	823.7	8.1
BESS-GFM	762.3	803.7	5.4

Table 4.2: Daily renewable curtailment with classical and proposed UC model.

	Classical UC [MWh]	**Proposed UC** [MWh]	**Difference** [%]
No BESS	7,586	8,386	10.6
BESS-GFL	5,415	6,762	24.9
BESS-GFM	5,415	6,136	13.3

Figure 4.6(a) presents the number of SGs committed across the case studies, while Figure 4.6(b) shows the percentage of SGs online for each generation technology. As observed in Figure 4.6(a), the number of committed SGs increase during daylight hours to accommodate the active power injection from renewables, particularly solar generation, which dominates the NG region. However, in some night hours, fewer SGs are committed in the scenarios with the proposed UC model. This is because larger units, such as coal units are preferred over OCGT and Diesel units, as they contribute more significantly to SCL. A similar trend is observed when comparing the BESS-GFL and BESS-GFM cases. In the BESS-GFL scenario, AFL violations are more pronounced, encouraging the commitment of coal units to contribute to base SCL in the network

throughout the day, while OCGT units are used for SCL peaking. In contrast, the BESS-GFM case exhibits smaller AFL shortfalls, allowing the model to reduce the dependence on coal units to provide base SCL. This reflects the contribution of GFM-BESS, which reduces the need for large coal units and enables more efficient UC.

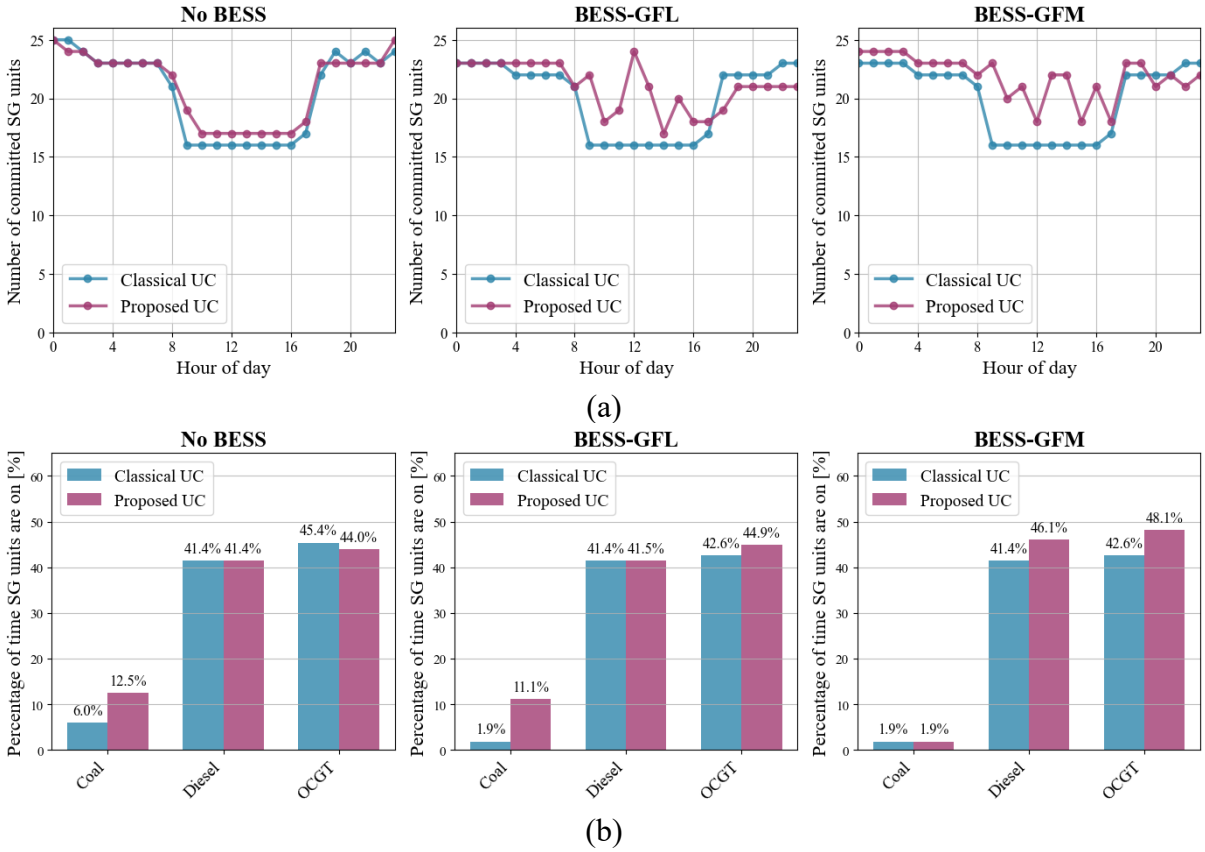


Figure 4.6: (a) Number of committed SGs for each case study. (b) Percentage of time SGs units are on by technology.

4.4 Impact of enabling AFL-driven curtailment

This section examines the impact of enabling renewable curtailment to satisfy AFL requirements. Many studies in the literature calculate system strength metrics using either the rated capacity of GFL-IBR units or the available active power based on renewable profiles. However, this approach can result in overly conservative UC decisions, leading to unnecessary increases in operating costs and renewable curtailment. To address this issue, Table 4.3 and Table 4.4 present the daily operating costs and curtailment levels under two conditions: considering the actual active power output of renewable GFL units (curtailment enabled) and the available power given by their renewable profiles (no curtailment enabled).

In the analysed cases, enabling curtailment to meet AFL requirements unlocks significant operational value. Specifically, total operating costs are reduced by around 5% in all scenarios. Interestingly, although it may seem counterintuitive, enabling curtailment also leads to an overall

reduction in daily renewable curtailment —by over 10% in all cases. This outcome is explained by the fact that, when curtailment is not allowed, the model must commit additional SGs to accommodate the expected active power injection from renewables. These SGs are then operated at their minimum stable level, which increases renewable curtailment. These results underscore the importance of considering the active power output of renewables when incorporating system strength constraints into operational models, as doing so can reduce both costs and total curtailment.

Table 4.3: Daily operating cost comparison with and without enabling AFL-driven curtailment.

	No curtailment enabled [k$]	**Curtailment enabled [k$]**	**Difference [%]**
No BESS	1,022.5	975.2	-4.6
BESS-GFL	845.8	823.7	-4.7
BESS-GFM	864.5	803.7	-5.0

Table 4.4: Daily renewable curtailment comparison with and without enabling AFL-driven curtailment.

	No curtailment enabled [MWh]	**Curtailment enabled [MWh]**	**Difference [%]**
No BESS	9,512	8,386	-13.4
BESS-GFL	7,444	6,762	-10.1
BESS-GFM	6,933	6,136	-13.0

Figure 4.7 illustrates the impact of enabling AFL-driven curtailment on the commitment of SGs. In the scenario without BESS, enabling curtailment reduces the overall number of committed units. In the BESS-GFL scenario, fewer OCGT units are committed, while the number of Diesel units increases. This occurs because OCGT units, with their larger capacities, provide more SCL to the system— what is needed when curtailment is not enabled. The effect becomes even more pronounced in the BESS-GFM case, where there is a significant reduction in committed coal units,

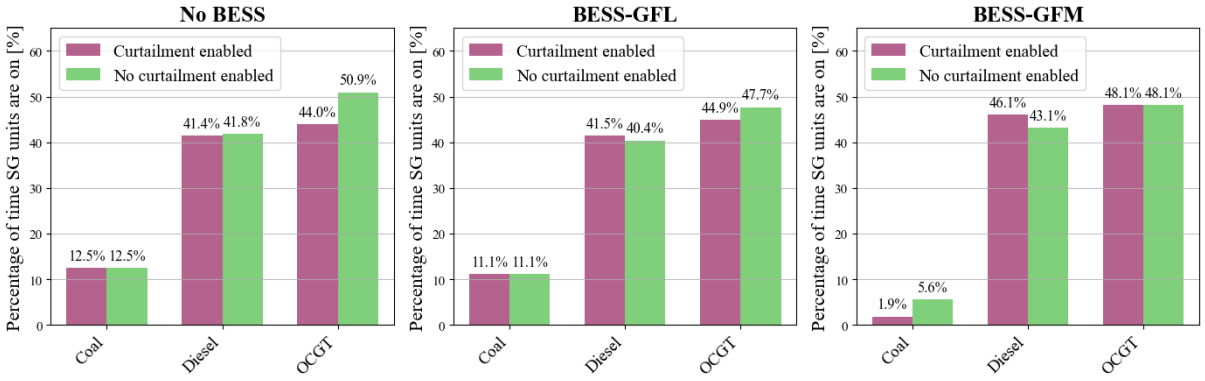


Figure 4.7: Percentage of time SGs units are on by technology comparison when enabling AFL-driven curtailment and without enabling it.

as base SCL provision is no longer necessary. This reduction is offset by an increase in Diesel units, which are smaller and more flexible, capable of supplying peak SCL. These findings highlight the importance of considering the active power output of renewables when incorporating system strength constraints into operational models, as doing so can replace the need for large, inflexible units with smaller, highly flexible ones.

4.5 Comparison with conventional security constraints

Section 2.2.1 discussed various strategies employed by system operators to maintain adequate levels of system strength. These strategies typically involve imposing operational constraints such as minimum inertia requirements, a minimum number of SGs online, or limits on non-synchronous penetration. While these measures help preserve system strength, they do not necessarily represent the most cost-effective approach. In this section, we compare these conventional practices with the proposed AFL-constrained UC model to highlight their differences and assess the potential benefits of the new methodology. The minimum inertia, minimum number of SGs online and maximum non-synchronous penetration constraints are defined in (4.1), (4.2) and (4.3), respectively.

$$\sum_{g \in G} u_{g,t} \mathrm{H}_g \mathrm{P}_g^{\max} \geq \mathrm{H}^{\min} \qquad \forall t \in T \quad (4.1)$$

$$\sum_{g \in G} u_{g,t} \geq \mathrm{G}^{\mathrm{on}} \qquad \forall t \in T \quad (4.2)$$

$$\frac{\sum_{r \in R} p_{r,t} + \sum_{b \in B} p_{b,t}^{\mathrm{dch}}}{\sum_{d \in D} \mathrm{D}_{d,t} + \sum_{b \in B} p_{b,t}^{\mathrm{ch}}} \leq \mathrm{NSP}^{\max} \qquad \forall t \in T \quad (4.3)$$

H_g represents the inertia (in seconds) of SG g, $\mathrm{H}^{\min}$ denotes the minimum inertia requirement, G^{on} indicates the required number of SGs online, and $\mathrm{NSP}^{\max}$ specifies the maximum allowable non-synchronous penetration.

Figure 4.8 presents the daily operating costs for the three constraints under different requirement levels in the BESS-GFL scenario. For comparison, the daily operating costs obtained with the proposed AFL-constrained UC model are also included in each plot (in red). The results demonstrate that the proposed model provides a more cost-effective approach to maintaining adequate system strength compared to the conventional security-constraints. Specifically, the AFL-constrained model achieves a daily operating cost of approximately 823.7 k$ while ensuring no AFL violations. In contrast, meeting the same objective with the minimum inertia, minimum number of SGs online and maximum non-synchronous penetration constraints, results in an operating cost of 876.8 k$, 949.2 k$ and 946.5 k$, respectively.

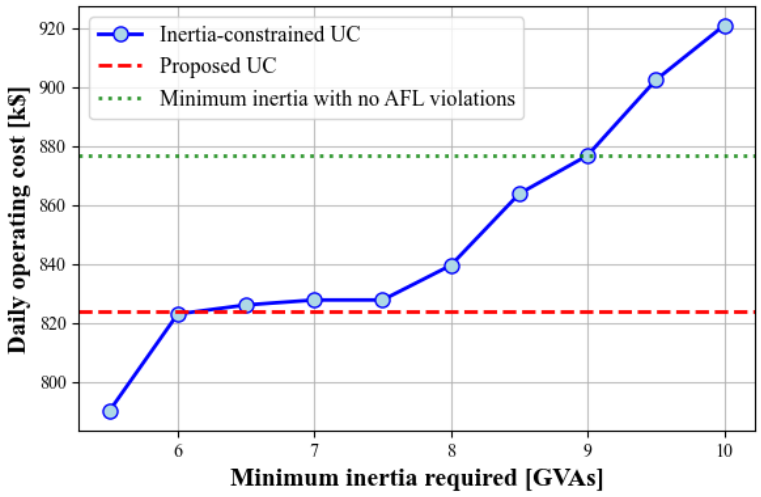
The cost difference between the cases involving the minimum inertia requirement and the minimum number of SGs online arises from two key factors. First, these constraints must be satisfied at every hour of the day, regardless of the active power injection from GFL-IBRs. Second, minimum inertia and minimum number of online SGs are system-wide requirements, whereas system strength depends on the SCL, which is a local characteristic specific to each bus.

Consequently, the AFL constraint enables targeted SG commitment to enhance SCL, where it is most needed. The cost difference is smaller in the case of the minimum inertia constraint because this requirement depends on the capacity of the SGs that must be committed. According to (4.1), the inertia contribution of SGs is linearly related to their capacity as well as their SCL contribution; therefore, SGs committed to supply inertia will also provide significant SCL (except in cases where SGs are equipped with flywheels to increase inertia). In contrast, the minimum number of SGs online tends to promote the commitment of smaller, more flexible SGs that do not significantly contribute to SCL.

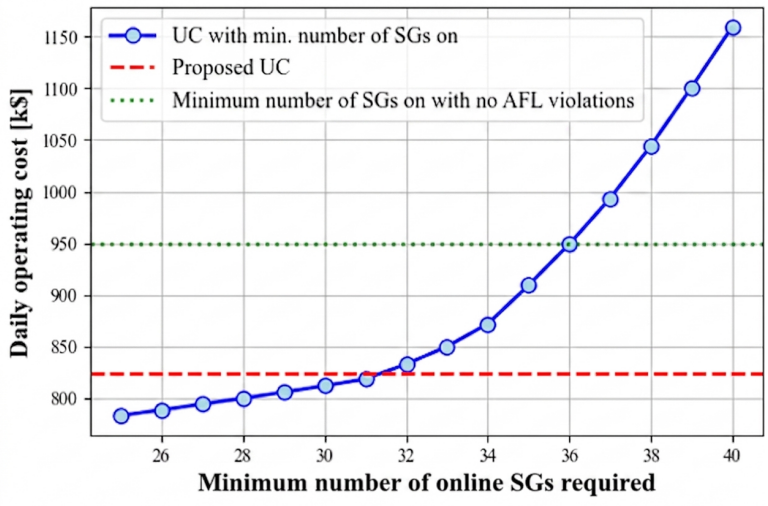
In comparison with the maximum non-synchronous penetration constraint, it is important to note that this requirement depends directly on the active power output from GFL-IBRs and completely disregards the dependency on SCL. As a result, this constraint primarily promotes active power curtailment from GFL-IBRs rather than the commitment of SGs. In fact, due to the high availability of solar resources, most SGs do not operate at their maximum capacity; therefore, enforcing this constraint tends to increase the dispatch of already committed SGs rather than requiring additional SG commitments. Furthermore, the maximum non-synchronous penetration constraint is also a system-wide requirement that does not account for the local nature of system strength. Ideally, this constraint should prioritize curtailment of GFL-IBRs connected to weak buses with low SCL. The findings in this section highlight the operational value of incorporating proper system strength constraints, as they enable more efficient and targeted solutions.

4.6 Analysis on future system scenarios

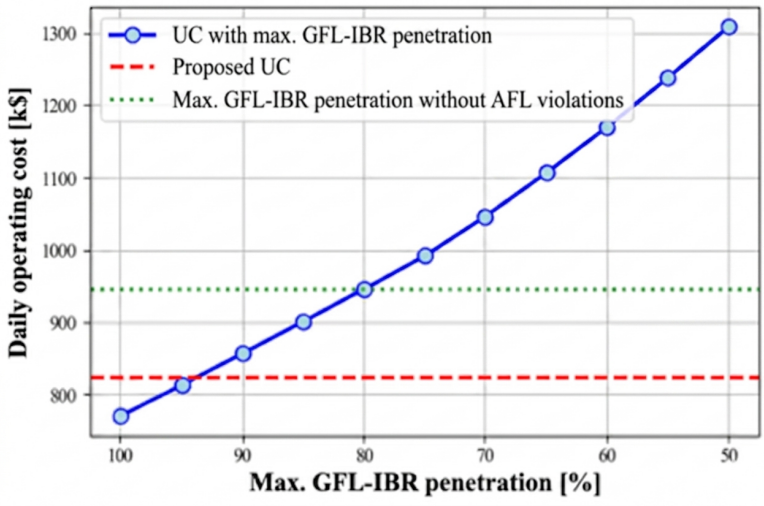
Driven by electrification trends and the declining CAPEX of PV panels and wind turbines, renewable penetration is expected to continue increasing in the coming decades. At the same time, coal generators are being progressively decommissioned due to decarbonization policies, which will likely lead to more frequent system strength shortfalls in future operational scenarios. To address this, the following section evaluates daily operating costs for different installed renewable capacities using the proposed model across different system scenarios: (i) coal generators remain in service, (ii) coal generators are fully decommissioned, and (iii) coal generators are replaced by synchronous condensers (SCs). For each scenario, five system configurations are analysed: No BESS, BESS-GFL, and BESS-GFM with varying SCL contributions (1.0 p.u., 1.5 p.u., and 2.0 p.u.).



(a)

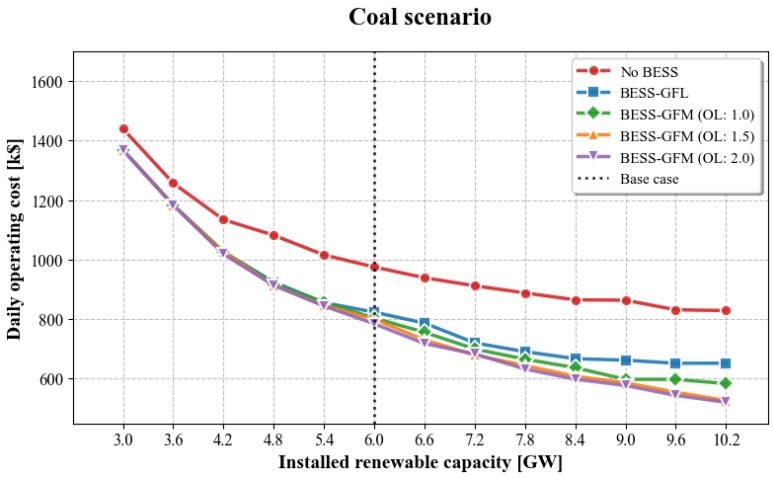


(b)

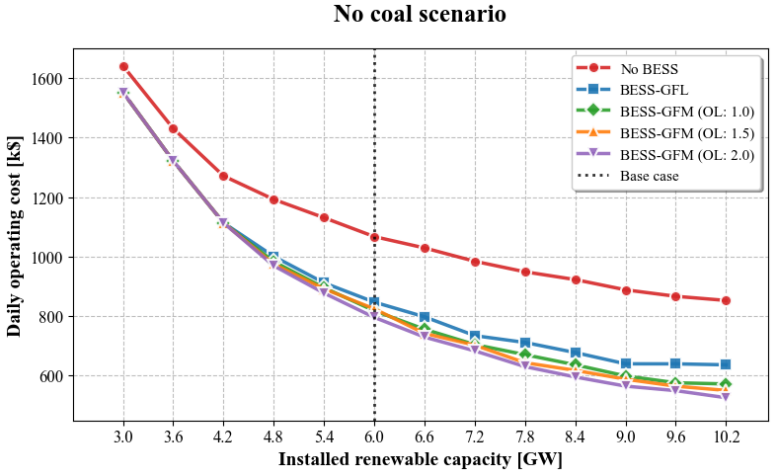


(c)

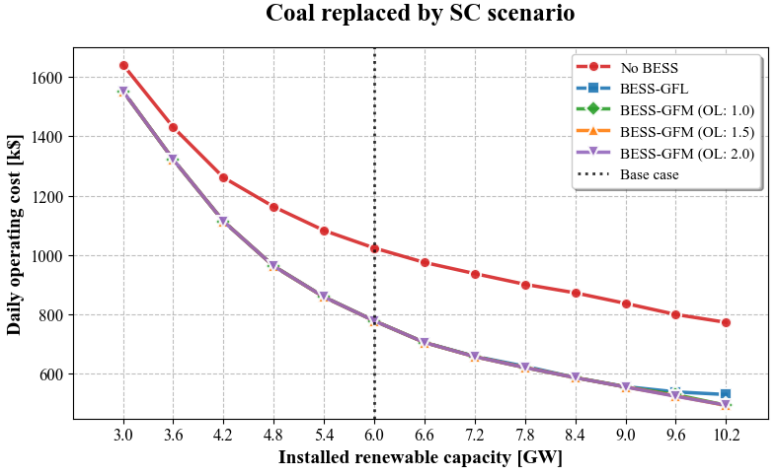
Figure 4.8: Daily operating cost for different conventional security-constraints. (a) Minimum inertia constraint. (b) Minimum number of online SGs required. (c) Maximum non-synchronous penetration.



(a)



(b)



(c)

Figure 4.9: Daily operating cost vs different levels of installed renewable capacity for different system configurations: No BESS (red line), BESS-GFL (blue line) and BESS-GFM with overloading capacity of 1.0 p.u. (green line), 1.5 p.u. (orange line) and 2.0 p.u. (purple line). (a) Scenario with coal-fired units. (b) Scenario with coal-fired units fully decommissioned. (c) Scenario with coal-fired units replaced by SCs.

Figure 4.9(a) shows the results of the scenario when coal generators remain in service. As renewable capacity increases, all system configurations exhibit a downward trend in daily operational costs, reflecting the economic benefits of higher renewable penetration, even when incorporating system strength constraints. However, the magnitude of cost reduction varies significantly across configurations. The "No BESS" scenario consistently incurs in the higher operational cost, underscoring the value of storage technologies in balancing the system. Moreover, after 7.0 GW of renewable penetration, the curve starts to saturate, indicating that the cost reduction in supplying demand with extra renewable power is similar to the added cost of committing units to host this extra renewable power. Among the BESS configurations, GFM-BESS outperform GFL-BESS, particularly at higher penetration levels, due to their ability to support system strength and reduce SG commitment. This highlights the importance of not only integrating storage but also ensuring its capability to support system strength through GFM operation, especially at higher renewable penetration levels. Increasing the GFM overload capacity beyond nominal levels results in additional cost savings; however, the improvement from 1.5 p.u. to 2.0 p.u. provides only marginal benefits, indicating diminishing returns.

Figure 4.9(b) presents the results for the scenario in which coal generators are fully decommissioned. The key difference compared to the scenario in Figure 4.9(a) lies in the increased value unlocked by GFM-BESS and its overloading capabilities. In the absence of coal generators, which traditionally supply large amounts of SCL, other devices must compensate for this requirement. Consequently, in this scenario, BESS-GFM with and overloading capacity of 2.0 p.u. achieves lower daily operating costs than BESS-GFM with an overloading capacity of 1.5 p.u.

Figure 4.9(c) presents the results for the scenario in which coal generators are replaced by SCs. These devices unlock significant operational value because they provide SCL without incurring fuel costs associated with active power generation. As a result, this scenario achieves the lowest daily operating cost at the highest renewable penetration level studied. However, since SCs supply the required SCL, differences between BESS configurations become negligible. In fact, variations between BESS-GFL and BESS-GFM cases are only noticeable at 10 GW of installed renewable capacity.

The findings from Figure 4.9 highlight the critical importance of incorporating system strength constraints when planning future power system scenarios. As coal-fired units are phased out, alternative sources of system strength must be integrated to maintain adequate levels while unlocking operational value. However, this integration requires careful planning to avoid unnecessary over-installation of assets —for example, scenarios where coal units are replaced by SCs, BESS-GFM configurations may fail to deliver additional cost savings.

4.7 Performance of the cut-generation algorithm

Finally, the performance of the cut-generation algorithm is analysed. The exact AFL-constrained UC formulation was attempted to solve. However, the matrices inversion involved $2 \cdot 72^2$ constraints (since there are 72 buses in the system) that, at the same time involve bilinear products. When attempting to solve the exact model, the process exceeded the available memory capacity. Then, the AFL-constrained UC model is solved using the cut-generation algorithm,

setting a maximum of 30 iterations and a violation tolerance of 10^{-6}. Table 4.5 shows the objective value and solving time in each iteration of the algorithm. It is concluded that the AFL-constrained UC model can be efficiently solved using the cut-generation algorithm. In fact, the model is solved under four minutes —a remarkably short time given the complexity of incorporating AFL requirements and the size of the system.

Table 4.5: Objective value and solving time obtained in each iteration when solving the AFL-constrained UC model using the cut-generation algorithm.

Iteration	Objective value [k$]	Solving time [s]	Accumulated solving time [s]
1	767.4	6.1	6.1
2	792.6	3.4	9.5
3	805.5	7.1	16.6
4	810.6	9.3	25.9
5	813.0	25.1	51.0
6	813.4	9.3	100.3
7	815.3	10.9	111.2
8	816.3	11.0	122.2
9	816.8	12.1	134.3
10	819.5	36.2	170.5
11	820.5	14.9	185.4
12	820.9	10.1	195.5
13	821.7	12.4	207.9
14	822.7	17.8	225.7
15	823.7	14.0	239.7

5 Conclusions

This work addressed the challenge of maintaining adequate system strength in power systems with high penetration of IBRs by incorporating system strength constraints into the day ahead planning problem. A UC model was developed that explicitly enforces system strength requirements using the AFL metric. Unlike conventional security constraints used imposed by system operators —such as minimum inertia, minimum number of online SGs, or limits on non-synchronous penetration— the AFL-based approach captures the local nature of system strength and accounts for the operating point of GFL-IBRs, consistently outperforming conventional approaches in terms of cost-effectiveness. For avoiding AFL violations during the studied day, the proposed model achieves daily operating cost reductions of up to 13% compared to constraints based on minimum inertia, minimum number of online SGs, or maximum non-synchronous penetration. These findings underscore the operational value of adopting system strength metrics that reflect local conditions rather than system-wide heuristics.

The inclusion of AFL-constraints introduces strong nonlinearities, making the UC problem a MINLP. To overcome this challenge, a cut-generation algorithm was proposed to iteratively approximate the original problem through linear cuts. Numerical results demonstrate that the algorithm solves the AFL-constrained UC efficiently, achieving convergence in under four minutes for a realistic representation of the NG region of the CPS.

Analyses under increasing renewable penetration and coal phase-out conditions confirm that system strength shortfalls will become more frequent and more severe in future grids. The proposed AFL-constrained UC methodology proves highly valuable in these scenarios by enabling cost-efficient solutions that maintain adequate levels of system strength. Results highlight the following insights: As coal-fired units are decommissioned, SCs and GFM-BESS become essential to compensate for SCL reductions. While increasing GFM-BESS overload capability (e.g., from 1.0 p.u. to 1.5 p.u.) significantly reduces operating, further increments beyond 1.5 p.u. yield marginal improvements (especially in the scenario where coal units are not decommissioned yet). Finally, excessive over-installation of system strength assets —such as SC combined with high capacity GFM-BESS— may fail to deliver additional cost-savings. This underscores the importance of integrated planning strategies that jointly consider system strength, renewable integration, and storage deployment to avoid unnecessary investments. Overall, these findings emphasize that future power systems require not only advanced operational models but also strategic coordination between technology adoption and system strength requirements to unlock maximum operational value.

5.1 Future work

While this research demonstrates the operational value of incorporating system strength constraints into day-ahead planning, several avenues remain open for future investigations. The current AFL-constrained UC model assumes deterministic forecasts for demand and renewable generation. However, real-world conditions are subject to significant uncertainty, particularly in systems with high penetration of variable renewable energy. Future research should incorporate

stochastic or robust optimization techniques to capture these uncertainties. This could involve scenario-based approaches, chance-constrained formulations, or distributionally robust models that ensure system strength requirements are met under a wide range of operating conditions. Additionally, probabilistic metrics for system strength —such as expected AFL or risk-based indices— could be developed to quantify the likelihood of violations and guide decision-making. Integrating uncertainty into the model would improve reliability and reduce the need for overly conservative commitments, unlocking further operational efficiency.

On the other hand, this work highlights the necessity of committing additional SGs to maintain system strength and demonstrates the operational value that assets such as GFM-BESS can unlock in meeting these requirements. Therefore, future work should explore how system strength requirements can be effectively integrated into electricity markets to align technical needs with economic signals. This includes developing locational pricing mechanisms that reflect the local nature of system strength, creating ancillary service markets for GFM capabilities, and adapting capacity markets to reward resources that provide short-circuit support. Additionally, dynamic procurement strategies could incentivize investments in technologies such as SCs and GFM-BESS. Finally, incorporating system strength considerations into renewable curtailment policies and locational marginal prices could minimize inefficiencies and promote secure, low-carbon operation.

Finally, this work focuses on short-term operational planning, but system strength challenges span multiple timeframes. Future research should explore integrated frameworks that co-optimize short-term unit commitment with medium- and long-term investment decisions. For example, planning models could jointly determine the optimal mix and location of SCs, GFM-BESS, and transmission reinforcements while considering operational constraints such as AFL. Such multi-horizon optimization would enable coordinated strategies that minimize total system costs across investment and operation, avoid asset over-installation, and ensure compliance with evolving system strength standards. Advanced decomposition techniques or hierarchical optimization approaches could be employed to maintain computational tractability for large-scale systems.

Bibliography

[1] Coordinador Eléctrico Nacional, “Reporte Energético - Abril 2025,” Santiago de Chile, Chile., 2025.

[2] Ministerio de Energía, “Estrategia de Descarbonización: Retiro y/o Reconversión de Unidades a Carbón,” Santiago, 2020.

[3] M. Ghazavi Dozein, B. Berry, J. V. Milanovic and P. Mancarella, “System Strength Beyond Fault Level,” *IEEE Access,* vol. 13, pp. 104184-104200, 2025.

[4] H. Gu, R. Yan and T. Saha, “Review of System Strength and Inertia Requirements for the National Electricity Market of Australia,” *CSEE Journal of Power and Energy Systems,* vol. 5, no. 3, pp. 295-305, 2019.

[5] North American Electric Reliability Corporation, “Short-Circuit Modeling and System Strength,” Atlanta, GA, USA, 2018.

[6] B. Bahrani, “Power-Synchronized Grid-Following Inverter Without a Phase-Locked Loop,” *IEEE Access,* vol. 9, pp. 112163-112176, 2021.

[7] J. Shair, H. Li, J. Hu and X. Xie, “Power system stability issues, classifications and research prospects in the context of high-penetration of renewables and power electronics,” *Renewable and Sustainable Energy Reviews,* vol. 145, p. 111111, 2021.

[8] Y. Zhu, T. Green, X. Zhou, Y. Li, D. Kong and Y. Gu, “Impedance Margin Ratio: a New Metric for Small-Signal System Strength,” *IEEE Transactions on Power Systems,* vol. 39, no. 6, pp. 7291-7303, 2024.

[9] Y. Wang, Y. Sun and S. Mei, “A method of distinguishing short-term voltage stability from rotor angle stability and its application,” in *2012 IEEE Innovative Smart Grid Technologies - Asia (ISGT Asia)*, Tianjin, 2012.

[10] North American Electric Reliability Corporation, “Integrating Inverter-Based Resources into Weak Power Systems,” Atlanta, GA, USA, 2017.

[11] N. Hatzargyriou, J. Milanovic, C. Rahmann, V. Ajjarapu, C. Canizares, I. Erlich, D. Hill, I. Hiskens, I. Kamwa, B. Pal, P. Purbeik, J. Sanchez-Gasca, A. Stankovic and T. Van Cutsem, “Definition and Classification of Power System Stability - Revisited & Extended,” *IEEE Transactions on Power Systems,* vol. 36, no. 4, pp. 3271-3281, 2021.

[12] D. Ortiz-Villalba, C. Rahmann, R. Alvarez, C. Canizares and C. Strunck, “Practical Framework for Frequency Stability Studies in Power Systems With Renewable Energy Sources,” *IEEE Access,* vol. 8, pp. 202286-202297, 2020.

[13] Coordinador Eléctrico Nacional, “Minuta DAOP N°04/2025 - Capacidad operacional del enlace 2x500 kV Nueva Pan de Azúcar - Polpaico con el seccionamiento de la línea 2x220 kV Quillota - Los Piuquenes en S/E Centella, en escenarios de alta generación ERV,” Santiago de Chile, Chile, 2025.

[14] Australian Energy Market Operator, "2024 Integrated System Plan (ISP)," 26 June 2024. [Online]. Available: https://aemo.com.au/energy-systems/major-publications/integrated-system-plan-isp/2024-integrated-system-plan-isp. [Accessed 4 April 2024].

[15] EirGrid, "System Non-Synchronous Penetration: Definition and Formulation," 2018.

[16] EirGrid, "Number of large fossil-fuel generators that must operate on Ireland's grid reduced," EirGrid, 11 April 2024. [Online]. Available: https://www.eirgrid.ie/news/number-large-fossil-fuel-generators-must-operate-irelands-grid-reduced. [Accessed 5 December 2025].

[17] O. Gomis-Bellmunt, J. Song, M. Cheah-Mane and E. Prieto-Araujo, "Steady-state impedance mapping in grids with power electronics: What is grid strength in modern power systems?," *International Journal of Electrical Power & Energy Systems,* vol. 136, p. 107635, 2022.

[18] IEEE/NERC Task Force on Short-Circuit and System Performance Impact of Inverter Based Generation, "Impact of Inverter Based Generation on Bulk Power System Dynamics and Short-Circuit Performance," IEEE, 2018.

[19] M. Nambiar and Z. Konstantinovic, "Impact of using synchronous condensers for power system stabiliy and improvement of short-circuit power in mining projects," *Mining Engineering,* vol. 67, no. 1, pp. 3-9, 2015.

[20] North American Electric Reliability Corporation, "Short-Circuit Modeling and System Strength," Atlanta, GA, USA, 2018.

[21] S.-H. Huang, J. Schmall, J. Conto, J. Adams, Y. Zhang and C. Carter, "Voltage Control Challenges on Weak Grids with High Penetration of Wind Generation: ERCOT Experience," in *2012 IEEE Power and Energy Society General Meeting*, San Diego, 2012.

[22] National Grid ESO, "System Operability Framework (SOF)," February 2022. [Online]. Available: https://www.neso.energy/publications/system-operability-framework-sof. [Accessed 09 October 2024].

[23] B. Vega, C. Rahmann, R. Álvarez and V. Vittal, "Determination of Control Requirements to Impose on CIG for Ensuring Frequency Stability of Low Inertia Power Systems," *IEEE Access,* vol. 10, 2022.

[24] CIGRÉ Brochure 370, "Integration of large scale wind generation using HVDC and power electronics," 2009.

[25] M. G. Taul, X. Wang, P. Davari and F. Blaabjerg, "Reduced-Order and Aggregated Modeling of Large-Signal Synchronization Stability for Multiconverter Systems," *IEEE Journal of Emerging and Selected Topics in Power Electronics,* vol. 9, no. 3, pp. 3150-3165, 2021.

[26] L. Fan and Z. Miao, "An Explanation of Oscillations Due to Wind Power Plants Weak Grid Interconnection," *IEEE Transactions on Sustainable Energy,* vol. 9, no. 1, pp. 488-490, 2018.

[27] M. Ghazavi Dozein, O. Gomis-Bellmunt and P. Macarella, "Simultaneous Provision of Dynamic Active and Reactive Power Response From Utility-Scale Battery Energy Storage Systems in Weak Grids," *IEEE Transactions on Power Systems,* vol. 36, no. 6, pp. 5548-5557, 2021.

[28] M. Gazhavi Dozein, B. C. Pal and P. Mancarella, "Dynamics of Inverter-Based Resources in Weak Distribution Grids," *IEEE Transactions on Power Systems,* vol. 37, no. 5, pp. 3682-3692, 2022.

[29] P. F. Mayer, M. Gordon, W.-C. Huang and C. Hardt, "Improving grid strength in a wide-area transmission system with grid forming inverters," *IET Generation, Transmission & Distribution,* vol. 17, no. 2, pp. 399-410, 2023.

[30] D. B. Rathnayake and B. Bahrani, "Multivariable Control Design for Grid-Forming Inverters With Decoupled Active and Reactive Power Loops," *IEEE Transactions on Power Electronics,* vol. 38, no. 2, pp. 1635-1649, 2023.

[31] R. Alijarrah, M. Karimi, R. Azizipanah-Abarghooee, Q. Salem and S. Alnaser, "Voltage dip propagation in renewable-rich power systems utilizing grid-forming converters," *IET Renewable Power Generation,* vol. 18, no. 5, pp. 753-763, 2024.

[32] S. Liaquat, M. F. Zia and M. Benbouzid, "Modeling and Formulation of Optimization Problems for Optimal Scheduling of Multi-Generation and Hybrid Energy Systems: Review and Recommendations," *Electronics,* vol. 10, no. 14, p. 1688, 2021.

[33] A. Gavrilovic, "AC/DC system strength as indicated by shor circuit ratio," in *International Conference on AC and DC Power Transmission*, London, UK, 1991.

[34] Y. Zhang, S.-H. Huang, J. Schmall, J. Conto, J. Billo and E. Rehman, "Evaluating system strength for large-scale wind plant integration," in *2014 IEEE PES General Meeting*, National Harbor, MD, USA, 2014.

[35] D. Wu, G. Li, M. Javadi, A. Malyscheff, M. Hong and J. N. Jiang, "Assessing Impact of Renewable Energy Integration on System Strength Using Site-Dependent Short Circuit Ratio," *IEEE Transactions on Sustainable Energy,* vol. 9, no. 3, pp. 1072-1080, 2018.

[36] W. Dong, H. Xin, D. Wu and L. Huang, "Small Signal Stability Analysis of Multi-Infeed Power Electronic Systems Based on Grid Strength Assessment," *IEEE Transactions on Power Systems,* vol. 34, no. 2, pp. 1393-1403, 2019.

[37] C. Yang, L. Huang, H. Xin and P. Ju, "Placing Grid-Forming Converters to Enhance Small Signal Stability of PLL-Integrated Power Systems," *IEEE Transactions on Power Systems,* vol. 36, no. 4, pp. 3563-3573, 2021.

[38] H. Xin, C. Liu, X. Chen, Y. Wang, E. Prieto-Araujo and L. Huang, "How Many Grid-Forming Converters Do We Need? a Perspective From Small Signal Stability and Power Grid Strength," *IEEE Transactions on Power Systems,* vol. 40, no. 1, pp. 623-625, 2025.

[39] CIGRÉ Working Group B4.62. TB 671, "Connection of wind farms to weak AC networks," CIGRÉ, 2016.

[40] Australian Energy Market Operator, "System Strength Impact Assessment Guidelines," 2023.

[41] EirGrid, SONI, "Annual Renewable Energy Constraint and Curtailment Report," 2025.

[42] Australian Energy Market Operator, "SA minimum synchronous generator requirements," 2023.

[43] Australian Energy Market Operator, "Reduction of Minimum Synchronous Generators in South Australia," 2025.

[44] ElectraNet, "Meeting System Strength Requirements in SA," 2025.

[45] H. Gu, R. Yan, T. K. Saha and E. Muljadi, "System Strength and Inertia Constrained Optimal Generator Dispatch Under High Renewable Penetration," *IEEE Transactions on Sustainable Energy,* vol. 11, no. 4, pp. 2392-2406, 2020.

[46] M. Gibbard and D. Vowles, "Simplified 14-Generator Model of the South East Australian Power System," The University of Adelaide, Adelaide, SA, Australia, 2014.

[47] Z. Chu and F. Teng, "Short Circuit Current Constrained UC in High IBG-Penetrated Power Systems," *IEEE Transactions on Power Systems,* vol. 36, no. 4, pp. 3776-3785, 2021.

[48] S. Urban, "McCormick envelopes," Cornell University, 12 December 2021. [Online]. Available: https://optimization.cbe.cornell.edu/index.php?title=McCormick_envelopes. [Accessed 10 June 2025].

[49] X. Zhang, Y. Liu, J. Zhao, J. Liu, M. Korkali and X. Chen, "Short-circuit current constrained unit commitment and transmission switching model for improving renewable integration: An MILP formulation," *IET Generation, Transmission & Distribution,* vol. 16, no. 9, pp. 1743-1755, 2022.

[50] Y.-K. Kim, S.-H. Lee and G.-S. Lee, "Strength-constrained unit commitment in IBR dominant power systems," *iEnergy,* vol. 4, no. 2, pp. 121-131, 2025.

[51] O. Alsac, B. Stott and W. F. Tinney, "Sparsity-Oriented Compensation Methods for Modified Network Solutions," *IEEE Transactions on Power Apparatus and Systems,* Vols. PAS-102, no. 5, pp. 1050-1060, 1983.

[52] L. Wu, M. Xu, J. Lin, H. Xu and L. Zheng, "Active Power Dispatch of Renewable Energy Power Systems Considering Multiple Renewable Energy Station Short-Circuit Ratio Constraints," *Electronics,* vol. 19, no. 13, p. 3811, 2024.

[53] S. Zhang, H. Zhang, H. Sheng, T. Huang and T. Zhao, “Optimal Operation of Renewable Energy Bases Considering Short-Circuit Ratio and Transient Overvoltage Constraints,” *Energies,* vol. 18, no. 5, p. 1256, 2025.

[54] Y. Lin, B. Wang, Q. Guo, H. Zhao and H. Sun, “Short-Circuit Ratio and Short-Term Voltage Security Constrained Unit Commitment in High Wind Power-Penetrated Power Systems,” *IEEE Transactions on Power Systems,* vol. 39, no. 4, pp. 5631-5644, 2024.

[55] Z. Chu and F. Teng, “Voltage Stability Constrained Unit Commitment in Power Systems With High Penetration of Inverter-Based Generators,” *IEEE Transactions on Power Systems,* vol. 38, no. 2, pp. 1572-1582, 2023.

[56] G. Cui, Z. Chu and F. Teng, “Control-mode as a Grid Service in Software-defined Power Grids: GFL vs GFM,” *IEEE Transactions on Power Systems,* vol. 40, no. 1, pp. 314-326, 2025.

[57] K. Van den Bergh, E. Delarue and W. D'haeseleer, “DC power flow in unit commitment models,” KU Leuven Energy Institute, 2014.

[58] R. A. Horn and F. Zhang, “Basic Properties of the Schur Complement,” in *The Schur Complement and Its Applications*, New York, NY, USA, Springer, 2005, pp. 17-46.

[59] S. Hadavi, J. Saunderson, A. Mehrizi-Sahni and B. Bahrani, “A Planning Method for Synchronous Condensers in Weak Grids Using Semi-Definite Optimization,” *IEEE Transactions on Power Systems,* vol. 38, no. 2, pp. 1632-1641, 2023.

[60] Coordinador Eléctrico Nacional, “Infotécnica,” [Online]. Available: https://infotecnica.coordinador.cl/. [Accessed 12 October 2025].

[61] Instituto Sistemas Complejos de Ingeniería, “Análisis costo/beneficio de potenciales trayectorias hacia una operación cero emisiones del Sistema Eléctrico Nacional,” Asociación Chilena de Energías Renovables y Almacenamiento, Santiago, Chile, 2025.

[62] M. Lubin, O. Dowson, J. Dias Garcia and J. Huchette, “JuMP 1.0: Recent improvements to a modelling language for mathematical optimization,” *Mathematical Programming Computation,* vol. 15, pp. 581-589, 2023.

[63] Gurobi Optimization, LLC, “Gurobi Optimizer Reference Manual,” 2024. [Online]. Available: https://www.gurobi.com/. [Accessed 4 August 2025].

[64] A. M. Kettner and M. Paolone, “On the Properties of the Power Systems Nodal Admittance Matrix,” *IEEE Transactions on Power Systems,* vol. 33, no. 1, pp. 1130-1131, 2018.

[65] D. Turizo and D. K. Molzahn, “Invertibility Conditions for the Admittance Matrices of Balanced Power Systems,” *IEEE Transactions on Power Systems,* vol. 38, no. 4, pp. 3841-3853, 2023.

Annexes

Annex A. PTDF matrix calculation

By assuming DC power flows, the active power flow in line l that connects buses i and j is given by (A.1).

$$f_l = b_l(\theta_i - \theta_j) \tag{A.1}$$

Where θ_i is the phase angle at bus i (in rads) and b_l is the susceptance of line l.

By defining the incidence matrix $\mathbf{C} \in \{-1,0,1\}^{\mathrm{L}\times\mathrm{N}}$ (L and N number of lines and buses, respectively) such that row l has +1 in the column of the origin bus i, -1 in the column of the end bus j, and zeros in the remaining columns. Then, for a line l which connects buses i and j, the angular difference these buses can be expressed as (A.2).

$$[\mathbf{C}\cdot\boldsymbol{\theta}]_l = \theta_i - \theta_j \tag{A.2}$$

Where $\boldsymbol{\theta} \in \mathbb{R}^{\mathrm{N}}$ is the vector of angles θ_i.

By defining the diagonal matrix of line susceptance as in (A.3), the vectorial relationship between flows and angles is given by (A.4). Then, the bus power injections are given by (A.5).

$$\mathbf{B}^{\mathrm{line}} = \mathrm{diag}(b_1, \dots, b_{\mathrm{L}}) \tag{A.3}$$

$$\mathbf{f} = \mathbf{B}^{\mathrm{line}}\cdot\mathbf{C}\cdot\boldsymbol{\theta} \tag{A.4}$$

$$\mathbf{p} = \mathbf{C}^{\mathrm{T}}\cdot\mathbf{B}^{\mathrm{line}}\cdot\mathbf{C}\cdot\boldsymbol{\theta} \tag{A.5}$$

Substituting the bus angles from (A.4) and (A.5) gives the DC power flow equation in (A.6), where $\mathbf{PTDF} \in \mathbb{R}^{\mathrm{L}\times\mathrm{N}}$ is defined in (A.7).

$$\mathbf{f} = \mathbf{PTDF}\cdot\mathbf{p} \tag{A.6}$$

$$\mathbf{PTDF} = \left(\mathbf{B}^{\mathrm{line}}\cdot\mathbf{C}\right)\cdot\left(\mathbf{C}^{\mathrm{T}}\cdot\mathbf{B}^{\mathrm{line}}\cdot\mathbf{C}\right)^{-\mathbf{1}} \tag{A.7}$$

The DC power flow equation for bus power balances (equation (A.5)) is linearly dependent. As a result, the matrix $\left(\mathbf{C}^{\mathrm{T}}\cdot\mathbf{B}^{\mathrm{line}}\cdot\mathbf{C}\right)$ is singular and its inverse does not exist. To overcome this issue, (at least) one node must be designated as reference node and removed from the DC power flow equations. In the matrix $\left(\mathbf{B}^{\mathrm{line}}\cdot\mathbf{C}\right)$ the column corresponding to the reference node must be removed while in the matrix $\left(\mathbf{C}^{\mathrm{T}}\cdot\mathbf{B}^{\mathrm{line}}\cdot\mathbf{C}\right)$ both the column and row corresponding to the reference node must be removed. With respect to voltage angles, only the difference in voltage angles between two neighbouring nodes matters. Therefore, the voltage angle of the reference node is set to zero. Finally, one additional relationship must be added to the set of equations to make

sure that the DC power flow has one unique solution. This relationship expresses that the sum of all nodal injections equals zero.

$$\sum_{i \in N} p_i = 0 \tag{A.8}$$

The PTDF matrix describes the linear relationship between the power injections in the grid ($\mathbf{p}$) and the active power flows through the transmission lines ($\mathbf{f}$). An element $[\mathbf{PTDF}]_{l,i}$ of the PTDF matrix gives the power flow through transmission line l caused by the injection of 1-unit active power at bus i and withdrawal of this active power at the reference bus. Due to the linear character of the PTDF matrix, the line flow at line l caused by an injection at bus i with withdrawal at bus j, can be written as the difference in the line flow l due to an injection at bus i with withdrawal at the reference node and the line flow in l due to an injection at bus j with withdrawal at the reference bus. In the final PTDF matrix, the column corresponding to the reference bus is a zero column.

Annex B. $\boldsymbol{Y^{GFM}}$ matrix properties

It can be concluded that $\boldsymbol{Y}^{\mathrm{GFM}}$ is a strictly positive definite matrix by the following result.

Lemma 1: $\boldsymbol{Y}^{\mathrm{GFM}}$ is a strictly positive definite matrix.

Proof: $\boldsymbol{Y}^{\mathrm{GFM}}$ can be expressed as (B.1).

$$\boldsymbol{Y}^{\mathrm{GFM}} = \mathbf{Y}^{0} + \mathrm{diag}\left(y_i^{\mathrm{GFM}}\right) \qquad \forall i \in N \quad \text{(B.1)}$$

$\mathbf{Y}^{0}$ is invertible in a power system with at least one voltage source connected to it [64], [65], then $\mathbf{Y}^{0}$ is strictly positive definite. Furthermore, since $\mathrm{diag}\left(y_i^{\mathrm{GFM}}\right)$ is positive semi-definite, then, from (B.1), $\boldsymbol{Y}^{\mathrm{GFM}}$ is strictly positive, completing the argument.

Annex C. Techno-economic parameters of SGs and BESS

Table C.1 and Table C.2 present the technical specifications and associated costs for the SGs. In these tables:

- **SGs 1-9** correspond to coal-fired generators, which have high capacity but are very inflexible, with minimum on/off times assumed to be 24 hours.
- **SGs 10-38** are diesel generators, characterized as small and highly flexible units, with minimum on/off times assumed to be zero.
- **SGs 39-41** represent geothermal generators, which have low variable costs but are very inflexible, with minimum on/off times of 24 hours.
- **SGs 42-50** are Open-Cycle Gas Turbines (OCGTs), which are less expensive than diesel generators and exhibit similar flexibility, with minimum on/off times ranging from 0 to 2 hours.
- **SG 51** corresponds to a thermosolar generator, with minimum on/off times of 8 hours.

Table C.1: Techno-economic parameters of existing SGs.

ID	Bus	C_g^V [$/MW]	C_g^{SU} [$]	C_g^{SD} [$]	P_g^{max} [MW]	P_g^{min} [MW]	R_g^U [MW/h]	R_g^D [MW/h]	X_g'' [p.u.]	Inertia [s]
1	12	75.0	135k	17.8k	177.0	70.0	107.0	107.0	0.275	7.57
2	4	323.3	48k	11.3k	267.5	51.7	215.8	215.8	0.221	3.19
3	4	327.9	48k	11.3k	271.6	51.7	219.9	219.9	0.516	4.8
4	15	60.2	53k	7.8k	266.0	85.0	181.0	181.0	0.225	3.86
5	15	59.7	53k	7.8k	266.0	85.0	181.0	181.0	0.325	3.86
6	12	76.2	135k	17.8k	165.0	45.2	120.0	120.0	0.230	2.5
7	45	55.8	73k	5.2k	377.0	74.3	302.7	302.7	0.287	7.57
8	45	184.9	67k	2.3k	165.9	40.0	125.9	125.9	0.205	4.10
9	45	180.0	94k	5.4k	175.0	41.5	133.5	133.5	0.300	4.10
10	53	216.1	6.6	6.6	51	0.0	2.0	2.0	0.285	3.26
11	20	153.5	229.0	6.2	6.0	0.0	6.0	6.0	0.259	0.38
12	20	153.5	229.0	6.2	6.0	0.0	6.0	6.0	0.42	6.13
13	20	154.8	229.4	6.3	6.5	0.0	6.5	6.5	0.434	2.50
14	20	158.8	313.3	11.2	134.1	0.0	13.0	13.0	0.272	3.00
15	22	270.8	49.7	9.4	6.3	1.0	5.3	5.3	0.291	0.78
16	22	268.7	22.4	2.9	1.5	0.5	1.0	1.0	0.341	4.48
17	22	262.4	33.3	3.7	1.9	1.0	0.9	0.9	0.341	4.48
18	20	316.8	199.5	260.8	9.0	5.0	18.5	18.5	0.294	0.79
19	20	343.3	258.1	211.9	17.7	0.0	17.7	17.7	0.246	4.80
20	20	454.1	665.8	332.6	33.3	0.0	33.3	33.3	0.278	6.38
21	20	472.9	351.8	550.4	36.0	0.0	36.0	36.0	0.278	6.38
22	30	338.2	4.9	3.4	3.0	10	2.0	2.0	0.303	2.85
23	43	222.3	11.2	15.2	27.9	10.0	17.9	17.9	0.330	6.59
24	21	422.0	3.8k	0.0	28.5	0.0	28.5	28.5	0.330	6.59
25	21	469.8	4.2k	0.0	10.0	0.0	26.0	26.0	0.300	4.00
26	21	373.2	252.2	97.0	7.7	0.0	7.7	7.7	0.292	2.18

The continuation of Table C.1 is found in Table C.2.

Table C.2: Techno-economic parameters of existing SGs (continuation)

ID	Bus	C_g^V [$/MW]	C_g^{SU} [$]	C_g^{SD} [$]	P_g^{max} [MW]	P_g^{min} [MW]	R_g^U [MW/h]	R_g^D [MW/h]	X_g'' [p.u.]	Inertia [s]
27	67	427.7	252.0	60.4	18.6	3.0	15.6	15.6	0.257	1.39
28	16	160.2	7.8k	689.0	6.7	2.0	4.7	4.7	0.300	2.26
29	16	162.1	7.8k	689.0	6.7	2.0	4.7	4.7	0.281	5.82
30	16	161.3	7.8k	689.0	6.7	2.0	4.7	4.7	0.365	4.05
31	16	172.5	7.8k	689.0	6.7	2.0	4.7	4.7	0.472	1.88
32	16	153.4	8.1k	915.1	6.7	2.0	4.7	4.7	0.302	5.50
33	16	128.4	8.1k	915.1	6.7	2.0	4.7	4.7	0.293	5.50
34	54	255.1	0.0	0.0	2.0	0.0	2.0	2.0	0.226	1.60
35	54	250.3	0.0	0.0	1.5	1.0	0.5	0.5	0.226	1.60
36	54	250.4	0.0	0.0	4.9	1.03	3.8	3.8	0.276	0.03
37	54	226.4	0.0	0.0	0.4	0.2	0.2	0.2	0.226	1.60
38	54	243.6	0.0	0.0	4.8	1.0	3.8	3.8	0.303	2.85
39	17	0.0	116.7	139.3	29.8	24.0	5.8	5.8	0.276	4.10
40	17	0.0	116.7	139.3	29.8	24.0	5.8	5.8	0.310	4.00
41	17	0.0	116.7	139.3	165.0	24.0	5.8	5.8	0.322	6.25
42	7	100.4	0.0	0.0	384.7	120.5	264.2	264.2	0.346	6.00
43	35	44.5	0.0	0.0	191.3	95.0	96.3	96.3	0.308	5.00
44	35	44.6	0.0	0.0	191.3	95.0	96.3	96.3	0.308	5.00
45	35	44.5	0.0	0.0	180.5	90.0	90.5	90.5	0.275	5.50
46	12	37.0	0.0	0.0	250.8	152.5	98.3	98.3	0.325	4.10
47	57	101.6	0.0	0.0	68.2	74.8	48.6	48.6	0.356	1.16
48	57	101.6	0.0	0.0.	100.5	74.8	46.7	46.7	0.272	0.46
49	70	36.2	108.4	7.0	400.0	117.0	283.0	283.0	0.784	5.50
50	69	37.6	108.4	7.0	37.5	13.9	23.6	23.6	0.364	5.50
51	29	0.9	440.8	531.8	12.0	10.0	100.0	100.0	0.257	1.39

Technical data for BESS is provided in Table C.3. For BESS operating in GFM mode, it is assumed that their subtransient effective impedance equals 1 p.u., allowing them to inject nominal fault current.

Table C.3: Technical parameters of BESS.

ID	Bus	E_b^{max} [MWh]	E_b^{min} [MWh]	E_b^{0} [MWh]	E_b^{T} [MWh]	$P_b^{dch,max}$ [MW]	$P_b^{ch,max}$ [MW]	η_b^{ch} [%]	η_b^{dch} [%]
1	6	9.8	0.49	5.1	5.1	2.45	2.45	97.5	97.5
2	2	404.4	20.2	212.3	212.3	101.1	101.1	97.5	97.5
3	2	561.8	28.1	294.9	294.9	140.5	140.5	97.5	97.5
4	2	212.0	10.6	111.3	111.3	53.0	53.0	97.5	97.5
5	10	192.0	9.6	100.8	100.8	48.0	48.0	97.5	97.5
6	19	180.0	9.0	94.5	94.5	45.0	45.0	97.5	97.5
7	21	36.0	1.8	18.9	18.9	9.0	9.0	97.5	97.5
8	20	217.6	10.88	114.24	114.24	54.4	54.4	97.5	97.5
9	66	304.0	15.2	159.6	159.6	76.0	76.0	97.5	97.5
10	30	13.16	0.6	6.9	6.9	3.3	3.3	97.5	97.5